



HAL
open science

Oxygen vacancies and tailored redox activity encountered with NiCo O nanostructures for promising applications in supercapacitor and water oxidation

Shusheel Kumar, Aneela Tahira, Adeel Liaquat Bhatti, Muhammad Ali Bhatti, Zaheer Ahmed Ujjan, Umair Aftab, Sooraj Kumar, Abdullah Al-Kahtani, Ayman Nafady, Elmuez Dawi, et al.

► To cite this version:

Shusheel Kumar, Aneela Tahira, Adeel Liaquat Bhatti, Muhammad Ali Bhatti, Zaheer Ahmed Ujjan, et al.. Oxygen vacancies and tailored redox activity encountered with NiCo O nanostructures for promising applications in supercapacitor and water oxidation. *Journal of Energy Storage*, 2024, 77, pp.109994. 10.1016/j.est.2023.109994 . hal-04377378

HAL Id: hal-04377378

<https://hal.univ-lorraine.fr/hal-04377378>

Submitted on 11 Jan 2024

HAL is a multi-disciplinary open access archive for the deposit and dissemination of scientific research documents, whether they are published or not. The documents may come from teaching and research institutions in France or abroad, or from public or private research centers.

L'archive ouverte pluridisciplinaire **HAL**, est destinée au dépôt et à la diffusion de documents scientifiques de niveau recherche, publiés ou non, émanant des établissements d'enseignement et de recherche français ou étrangers, des laboratoires publics ou privés.

1 **Oxygen vacancies and tailored redox activity encountered with NiCo₂O₄ nanostructures**
2 **for promising applications in supercapacitor and water oxidation**

3 Shusheel Kumar^a, Aneela Tahira^c, Adeel Liaquat Bhatti^a, Muhammad Ali Bhatti^d, Zaheer Ahmed
4 Ujjan^a, Umair Aftab^c, Sooraj Kumar^j, Abdullah A. Al-Kahtani^h, Ayman Nafady^h, Elmuez Dawiⁱ,
5 Mélanie Emo^f, Brigitte Vigolo^f, Antonia Infantes-Molina^g, Zafar Hussain Ibupoto^{b*}

6
7
8 ^a*Institute of Physics, University of Sindh Jamshoro, 76080, Sindh, Pakistan.*

9 ^b*Institute of Chemistry, University of Sindh Jamshoro, 76080, Sindh, Pakistan.*

10 ^c*Institute of Chemistry, Shah Abdul Latif University Khairpur Mirs, Sindh, Pakistan.*

11 ^d*Institute of Environmental Sciences, University of Sindh Jamshoro, 76080, Sindh, Pakistan.*

12 ^e*Mehran University of Engineering and Technology, 7680 Jamshoro, Sindh, Pakistan.*

13 ^f*Université de Lorraine, CNRS, IJL, F-54000 Nancy, France.*

14 ^g*Department of Inorganic Chemistry, Crystallography and Mineralogy, Unidad Asociada al ICP-
15 CSIC, Faculty of Sciences, University of Malaga, Campus de Teatinos, 29071, Malaga, Spain.*

16 ^h*Chemistry Department, College of Science, King Saud University, Riyadh, 11451, Saudi Arabia.*

17 ⁱ*College of Humanities and Sciences, department of Mathematics and Sciences, Ajman University,
18 P.O. Box 346, United Arab Emirates.*

19 ^j*Department of Chemical Engineering, Mehran University of Engineering and Technology, 7680
20 Jamshoro, Sindh, Pakistan*

21 ^{*}*Corresponding author(s): Zafar Hussain Ibupoto, PhD*

22 *Email : zaffar.ibhupoto@usindh.edu.pk*

23
24 **Abstract**

25 It is well known that transition metal oxides play a significant role in the development of
26 efficient electrochemical energy storage and conversion systems. However, their application
27 is limited by low electrical conductivity, a limited number of electroactive sites, and limited
28 stability. A study is presented in which sustainable development goals (SDGs) are used for
29 the synthesis of new materials using green reducing, capping, and stabilizing agents, which
30 minimizes environmental pollution. NiCo₂O₄ nanostructures were prepared using orange peel
31 extract and its fruit juice in order to demonstrate the ability of these green chemical
32 components to manipulate NiCo₂O₄'s structural and functional properties. In order to achieve
33 this goal, 1 mL and 2 mL of either orange peel extract or fruit juice were used in order to

34 produce heterogeneous nanoparticles of NiCo₂O₄. The electrochemical supercapacitor
35 prepared with the as-prepared NiCo₂O₄ nanostructures with 1 mL of orange peel extract
36 showed a specific capacitance of 997.50 Fg⁻¹ with a cycling stability of more than thirty
37 thousand cycles, resulting in a capacitance retention rate of almost 100% at 1.5 Ag⁻¹. In
38 addition, during the oxygen evolution reaction (OER), the overpotential was 120 mV at 20
39 mA/cm² and the Tafel slope was 110 mVdec⁻¹, with a prolonged stability exceeding 45 h.
40 With an electrode material comprising NiCo₂O₄ nanostructures and an orange peel extract,
41 outstanding electrochemical performance was obtained. This could be explained by several
42 factors, including high electroactive site exposure, rapid charge transfer kinetics, high
43 hydroxide adsorption, oxygen vacancies on the surface, and abundance of Co(III). The
44 approach described here can be used for the facile synthesis of a wide range of
45 nanostructured functional materials that exhibit impressive electrochemical properties,
46 particularly for energy storage and conversion applications.

47

48 **Keywords:** Orange peel extract, Orange fruit juice, NiCo₂O₄ nanostructures, Low temperature
49 sintering, Supercapacitor, Oxygen evolution reaction.

50

51 **1. Introduction**

52 With the current global challenges pertaining to renewable energy sources and energy storage
53 devices for electronics, wearables, and vehicles [1, 2], researchers have been motivated to
54 develop efficient energy storage and conversion systems. Due to their high cycling stability
55 and power density, supercapacitors are highly emerging as energy storage systems [3, 4]. A
56 supercapacitor works by adsorbing ions from electrolytic solutions onto the electrode
57 material [5]. Supercapacitors are unique in that they can be manufactured using highly
58 durable electrode materials that provide excellent capacitance [6]. In recent years,
59 electrochemical supercapacitors have gained importance owing to their fast charge-discharge
60 rate and low cost [7-9]. Even so, their low specific energy indicates that they are not suitable
61 for a wide variety of applications. The development of supercapacitors has been largely
62 powered by battery-type electrode materials, which have been found to provide high energy
63 storage through a well-defined redox process. It is always sought after that electrode
64 materials in this field have a high surface area and enough space for electron capture in order

65 to achieve high electrochemical activity [10]. Among the bimetallic oxides, nickel-cobalt
66 oxide (NiCo_2O_4) nanostructures are highly popular because they possess a higher
67 conductivity than ZnFe_2O_4 , CoMoO_4 , MnMoO_4 , $\text{Zn}_3\text{V}_2\text{O}_8$, or NiMnO_3 [11-13]. NiCo_2O_4
68 offers improved redox properties, as well as environmental conservation, cost effectiveness,
69 and chemical inertness [14, 15]. It is also considered to be a highly active cathode material
70 for Zn-based batteries due to its excellent reversibility and capacity exceeding 500 mAh/g
71 [16]. Despite the practical specific capacitance and rapid kinetics, NiCo_2O_4 nanostructures
72 are far from commercial use due to its insignificant electroactive sites and poor electrical
73 conductivity[17-19]. A variety of methods have been employed to synthesize spinel NiCo_2O_4
74 nanostructures, including sol-gel deposition, hydrothermal deposition, and electrochemical
75 deposition [20, 21, 22]. The majority of metal oxide nanostructures are prepared physically
76 and chemically, involving hazardous and active reducing compounds such as sodium
77 borohydride and hydrazine hydrate, which have adverse effects on the environment and
78 biological systems [23, 24]. Nanostructured materials can be synthesized using physical
79 techniques that produce heterogeneous nanoparticles with substantial energy [25]. The
80 United Nations have been formulated Sustainable Development Goals (SDGs) about the
81 synthesis of new chemical compounds with negligible effect on the environment [26, 27]. For
82 these reasons, recently, there has been considerable attention paid to preparing nanostructured
83 materials using green methods and demonstrating the process of synthesizing nanostructured
84 materials using biological methods [28-31] Consequently, the researchers developed easy,
85 low-cost, reliable, and eco-friendly methods for preparing nanostructured materials [32, 33].
86 Thus, scientists have been able to synthesize highly stable nanostructured materials that are
87 functionally oriented by utilizing a variety of biological resources, including viruses, yeast,
88 fungi, seaweed, microalgae, actinomycetes, plant extracts, agricultural waste, horticultural
89 food materials, bacteria, and discarded food materials [34, 35]. The simplicity and safety of
90 these biological methods for producing nanostructures make them particularly attractive.

91 As part of our efforts to contribute to the Sustainable Development Goals, we have developed
92 NiCo_2O_4 and Co_3O_4 nanostructured materials for the conversion and storage of energy [36-
93 38]. It is evident from the literature that NiCo_2O_4 nanostructures synthesis by biological
94 means has less likely been studied than chemical methods. Previously, we synthesized
95 NiCo_2O_4 nanostructures from biomass wastes. These nanostructures were then deposited
96 directly onto glassy carbon electrodes for capacitance and oxygen evolution [36, 37]. A wide
97 range of green chemical compounds in orange peel extract and its fruit juice can enhance the

98 electrochemical properties of nanostructured materials for energy conversion and storage. In
99 2014, oranges produced approximately 89 million tons of juice worldwide [38]. About 26%
100 of citrus fruits are processed into citrus juice in industry, and approximately 15 billion tons of
101 citrus waste are produced every year and different varieties of citrus fruits have been
102 harvested around the world [39 - 44].

103 Orange peel extracts and fruit juice provide an attractive green reducing, capping, and
104 stabilizing agent for the synthesis of high-performance nanostructured materials. In our
105 experience, no literature has been found that describes the use of orange peel biomass waste
106 as a source of NiCo_2O_4 nanostructures. In addition, there has never been a study that
107 compares peel extracts with fruit juices from the same plant. Green chemistry of reducing,
108 stabilizing, and capping agents differs significantly between peel extracts and fruit juice,
109 which affects NiCo_2O_4 nanostructure shape, electrical conductivity, and surface properties,
110 resulting in different electrochemical energy storage and conversion results. As of yet, no
111 studies have been conducted on the synthesis of NiCo_2O_4 nanostructures from orange peels
112 and their juices for the enhancement of capacitance and oxygen evolution reactions.
113 Previously, no report has been published on the design of electrode materials based on
114 NiCo_2O_4 nanostructures deposited on nickel foam using sintering and assisted by biomass
115 waste.

116 **2. Materials and Methods**

117 **2.1. Chemical reagents**

118 Sigma Aldrich, Karachi, Sindh, Pakistan, provided high quality analytical grade cobalt
119 chloride hexahydrate (98%), urea 99% ($\text{N}_2\text{H}_4\text{CO}$), potassium hydroxide 90% (KOH),
120 methanol 98%, isopropanol 99%, 5% Nafion, and nickel chloride hexahydrate 98% (NiCl_2
121 $6\text{H}_2\text{O}$). An orange fruit was purchased from a local market in Hyderabad, Sindh, Pakistan.
122 Deionized water was used to prepare the desired solutions.

123 **2.2. Preparation of NiCo_2O_4 nanostructures using orange peel extract and its fruit juice**

124 NiCo_2O_4 nanostructures were prepared using a hydrothermal method without (referred to as
125 pure NiCo_2O_4) and with orange peel extract and fruit juice: fresh orange fruit was washed
126 with deionized water several times to remove particles from the peel surface, then dried.
127 Afterward, the orange peel was removed along with the white fibrous material. Orange peel
128 slices were chipped into small pieces and ground into juicer machines. A liquid was obtained

129 from orange peel by filtering through filter paper. Filtrate was collected and stored in a
130 refrigerator at 4 °C. In the meantime, orange juice was collected in the juicer machine and
131 filtered through filter paper, and stored at 4 °C in the refrigerator. Hydrothermal growth of
132 NiCo₂O₄ nanostructures at 95 °C for 5 h in a preheated electric oven started with 0.1 M
133 cobalt chloride hexahydrate, 0.015 M nickel chloride hexahydrate, and 0.1 M urea in 100 mL
134 of deionized water. The pH of the nickel-cobalt precursor solution was about 6.71. An
135 aluminum sheet was tightly wrapped around the growing solution to prevent evaporation.
136 Bimetallic hydroxide was then combusted at 500 °C for five hours after hydrothermal
137 treatment. NiCo₂O₄ nanostructures were then formed into a bimetallic black oxide phase. In
138 contrast, the orange peel extract and its fruit juice mediated synthesis of NiCo₂O₄
139 nanostructures used the same precursors but used 1 mL and 2 mL of each for hydrothermal
140 annealing and thermal annealing. The bimetallic nickel-cobalt oxides prepared with 1 and 2
141 mL of orange peel extract and with 1 and 2 mL of orange juice are named op-1, op-2, or-1
142 and or-2, respectively. With the addition of 1 mL and 2 mL of orange peel extract, the pH of
143 the nickel-cobalt precursor solution was slightly changed from 6.45 to 6.23, whereas the pH
144 change with orange juice was 6.31 to 5.97.

145 **2.3. Structural investigations on the green mediated synthesis of various NiCo₂O₄** 146 **nanostructures**

147 A variety of analytical techniques were used to study the structural properties of NiCo₂O₄
148 nanostructures derived from orange peel extract and fruit juice. The objective of the structural
149 studies was to gain a better understanding of the material morphology, the crystalline
150 properties, the surface chemical composition, and the crystal facets. In order to accomplish
151 this, the morphology of the samples was analyzed via Scanning Electron Microscopy (SEM)
152 at an accelerated voltage of 2 kV, using a ZEISS Gemini SEM 500 linked to a field emission
153 gun. The crystal arrays were explored by Powder X-Ray Diffraction (PXRD) under the
154 experimental measurement set up of X-rays of wavelength of $\lambda K\alpha = 1.5406 \text{ \AA}$ generated by a
155 Cu anode operating at 45 kV and 45 mA. Transmission Electron Microscopy (TEM) and
156 Scanning Transmission Electron Microscopy (STEM) measurements were conducted with a
157 JEOL JEM-ARM 200F Cold FEG microscope operating at 200 kV and equipped with a probe
158 corrector (Cs). An energy dispersive X-ray spectrometer (SDD, Joel DRY SD 30 GV) was
159 used to collect chemical information. The surface chemical composition was obtained by
160 applying X-ray photoelectron spectroscopy (XPS) with a Scienta ESCA 200 Spectrometer at

161 low operating pressure (10-10 mbar) and under ultrahigh vacuum using a monochromatic Al
162 K α X-ray source. The recorded binding energies of different NiCo₂O₄ nanostructures
163 based on orange peel extract and fruit juice were well matched to a reference binding energy
164 of 284.6 eV measured for the C1s peak.

165 **2.4. Electrochemical characterization of various NiCo₂O₄ nanostructures using** 166 **biomasses of orange peel extract and its fruit juice**

167 In order to investigate electrochemical applications such as supercapacitors and oxygen
168 evolution reactions, the effects of orange peel extracts and their fruit juices on NiCo₂O₄
169 nanostructures have been investigated at different electrolytic concentrations of KOH. Before
170 electrochemical testing, a slurry containing various NiCo₂O₄ nanostructures was prepared in a
171 3:1 ratio using deionized water/ethanol and 5 mg of each material. Following this, 100 μ L of
172 5% Nafion were added to the catalyst slurry ink for 20 minutes, followed by magnetic
173 stirring. Then, 2 cm² of cleaned nickel foam was deposited with each slurry of catalytic
174 material 5 times via a dip coating and drying process. Nanostructured NiCo₂O₄ and nickel
175 foam electrodes were sintered at 70 °C for 30 minutes in an electric oven. As a result,
176 electrochemical measurements could be performed on electrode materials. Calomel
177 (Hg/HgO) electrodes are used as reference electrodes, and graphite rods serve as counter
178 electrodes. Using chronopotentiometry, electrochemical supercapacitors were studied in 3.0
179 M KOH for the recording of galvanostatic charge-discharge curves (GCDs) for the
180 calculation of specific capacitances (Cs), energy densities, power densities, cycling stability,
181 and columbic efficiency [19]. For each electrode material, cyclic voltammetry (CV) was
182 utilized to assess its redox behavior. Electrochemical impedance spectroscopy (EIS) was
183 conducted at 100 kHz to 0.1 Hz utilizing an amplitude of 10 mV and biasing an onset
184 potential for the OER. Linear sweep voltammetry (LSV) was used to measure oxygen
185 evolution reactions (OER) in 1.0 M KOH solution at a scan rate of 2 mV/s. An estimation of
186 the electrochemical active surface area (ECSA) was made using CV curves in a non-Faradic
187 region at different scan rates. A chronoamperometric study was conducted on an OER
188 overpotential to determine its durability.

189 **3. Results and discussion**

190 **3.1. Structural and compositional characterization of as prepared NiCo₂O₄** 191 **nanostructures using orange peel extract and its fruit juice**

192 The powder XRD analysis of NiCo₂O₄ nanostructures prepared with orange peel extract and
193 its fruit juice is shown in Figure 1a. Nanostructures of NiCo₂O₄ exhibited Miller indices of
194 (111), (220), (311), (222), (400), (422), (511) and (440), corresponding to 18.9^o , 31.2^o ,
195 36.7^o , 38.4^o , 46.7^o , 55.4^o , 59.1^o and 65.0^o , respectively. Using the standard JCPDS card
196 number 01-073-1702, all of these measured reflections are characteristic of NiCo₂O₄
197 nanostructures in the spinel phase. NiCo₂O₄ nanostructures prepared using orange peel
198 extract and juice fruit showed similar XRD spectra as pure NiCo₂O₄ nanostructures with
199 spinel structure and cubic phase (Figure 1a). Compared to pure NiCo₂O₄ nanostructures,
200 orange peel extract and fruit juice had a different relative intensity of reflections, indicating
201 that they contained a wide range of reducing, capping, and stabilizing agents. Furthermore,
202 orange peel extract and juice showed varying relative intensities, indicating that reducing,
203 capping, and stabilizing agents were present in different amounts. According to an XRD
204 analysis, orange peel extract and fruit juice have significant effects on NiCo₂O₄
205 nanostructures regarding crystalline properties, due to the presence of several green reducing,
206 capping, and stabilizing agents that also enhance energy storage and conversion. In Figure 1a,
207 NiCo₂O₄ nanostructures prepared from orange peel and juice fruit biomass were examined by
208 scanning electron microscopy and compared with pure NiCo₂O₄ nanostructures. (Figure 1b
209 and insert). In contrast, NiCo₂O₄ nanostructures prepared with orange peel extract and fruit
210 juice (Op and or samples, respectively) show randomly arranged nanoparticles. This indicates
211 that the green reducing, capping, and stabilizing agents play a dynamic role in changing
212 nanowires from organized nanowires into disorganized nanoparticles at both concentrations;
213 for example, 1mL and 2mL (Figures 1c-1f and inserts). The individual nanoparticle size is as
214 well dramatically reduced from around 50 nm in NiCo₂O₄ prepared without Biosource agent
215 down to around 10 nm from SEM and TEM imaging. The possible morphological
216 transformation could be caused by changes in the pH of the growth solution, as described in
217 the experimental section. As a result, the growth solution became more acidic than orange
218 peel extract or juice (p = 0.5 or 0.7 unit pH reduction compared to the solution without the
219 bio-sourced additives). Since a relatively weak pH change has resulted in significant changes
220 in NiCo₂O₄ morphology, the pH conditions may play an important role in the structural and
221 morphological changes. During the growth process, the nickel and cobalt ions could be
222 coordinated by lone pair atoms in the green compounds of orange peel extract and its fruit
223 juice. Due to this, there may be different mechanisms involved by the use of orange peel
224 extract and its fruit juice compared to the synthesis mechanism using no additives at all. The

225 Scheme 3 illustrates the morphological transformation in brief. As a result of SEM analysis, it
226 is evident that orange peel extract and its fruit juice produce nanoparticles of different sizes
227 and surfaces, suggesting that orange peel extract contains fewer green reducing, capping and
228 stabilizing agents than fruit juice. Consequently, the amount of these green chemical
229 compounds in biomass may have a different impact on the shape orientation of
230 nanostructured materials.

231 As part of this study, the morphology, crystal structure, and chemical composition of orange
232 peel extract assisted NiCo₂O₄ nanostructures were examined by means of High Resolution
233 Transmission Electron Microscopy (HRTEM) and Scanning Transmission Electron
234 Microscopy (STEM) coupled with energy dispersive X-ray spectroscopy (EDXS).
235 Nanostructures of NiCo₂O₄ mediated by orange peel extract were composed of nanoparticle
236 clusters that were less than 50 nanometers in size (Figures 2a-b), while pure NiCo₂O₄
237 nanostructures were composed of nanoparticles that were 20 to 80 nanometers in size
238 assembled into nanorods [36]. Figures 2c-e demonstrate Ni, Co, and O elements in these
239 orange peel-mediated NiCo₂O₄ nanostructures without any other impurities. Fast Fourier
240 Transform exhibits spots at 2.8, 2.0 and 1.4 Å (insert of Figure 2b), corresponding to (022),
241 (040) and (044) reflections of the Fd-3m cubic structure of NiCo₂O₄ (a = 8.1 Å) respectively,
242 as already observed with XRD analysis. In addition to SEM and XRD, TEM and STEM
243 results confirmed these observations. Citrus peel extract inhibits the formation of nanowires
244 based on self-assembly of nanoparticles while promoting the formation of smaller aggregates
245 of NiCo₂O₄.

246 An XPS analysis was performed to obtain a deep understanding of the chemical state of Ni
247 and Co ions, as well as to evaluate the surface chemical composition of NiCo₂O₄
248 nanostructures prepared with orange peel extract and its fruit juice (Figure 3). Orange peel
249 extract assisted synthesized NiCo₂O₄ nanostructure (Op-1) exhibits Co 2p_{3/2} contributions at
250 779.4 eV for Co III and 781.4 eV for Co II, as well as satellite peaks at 784.2 and 788.0 eV;
251 Figure 3a, which are in accordance with previous studies [45-47]. Additionally, the Ni 2p_{3/2}
252 signal (Figure 3ba) was decomposed at various binding energies, including 854.1 eV for
253 Ni(II), 855.7 eV for Ni(III), and 857.3 eV for Ni(OH) as well as the satellite peak at 861.37
254 eV [48]. Ni²⁺/Ni³⁺ and Co²⁺/Co³⁺ atomic ratios were estimated to be 0.70 and 0.75,
255 respectively. The orange fruit juice mediated NiCo₂O₄ nanostructure (Or-1) was also
256 investigated, and similar Co 2p_{3/2} and Ni 2p_{3/2} spectra were observed as shown in Figure 3a,b.

257 The corresponding $\text{Ni}^{2+}/\text{Ni}^{3+}$ and $\text{Co}^{2+}/\text{Co}^{3+}$ atomic ratios were 0.84 and 0.71 respectively,
258 indicating that a higher surface concentration of Ni^{2+} and Co^{3+} species was present in the
259 orange fruit juice-based sample. Based on this analysis, it was demonstrated that the surface
260 aspects of NiCo_2O_4 nanostructures were strongly influenced by the relative content of green
261 reducing, capping, and stabilizing agents derived from orange peel extracts and fruit juices.
262 Compared to the orange juiced-mediated NiCo_2O_4 nanostructures, the orange peel extract
263 revealed a relatively higher amount of Co^{3+} ions on the surface, which contributed to their
264 electrochemical performance [50]. After examining the O 1s spectra of orange peel extracts
265 and fruit juice-mediated NiCo_2O_4 nanostructures (Figure 3c), three principal attributions were
266 identified at 529.5 eV, 531.3 eV, and 532.8 eV, and 529.3 eV, 531.0 eV, 532.5 eV which could
267 be attributed to *OLat*, *OSur*, and *OChe*, respectively. As previously reported [45], *OLat*
268 corresponds to the lattice oxygen in metal-oxygen chemical bonds, while *OSur* corresponds
269 to surface defects and oxygen vacancies, and *OChe* to chemisorbed oxygen. There is
270 substantial variation in the amount of oxygen species present in orange peel extract and fruit-
271 mediated NiCo_2O_4 nanostructures, with the orange peel extract sample having a higher
272 proportion of surface vacancies. As prepared NiCo_2O_4 nanostructures using biomasses of
273 orange peel extract and juice, their major contributions towards enhanced electrochemical
274 activity could be tested further.

275 **3.2. Evaluation of electrochemical supercapacitor performance of different NiCo_2O_4** 276 **nanostructures prepared with orange peel extract and its fruit juice.**

277 Prior to electrochemical measurements, NiCo_2O_4 nanostructures were deposited onto nickel
278 foam with a diameter of 1 cm^2 and sintering at low temperatures. The cyclic voltammetry
279 (CV) of orange peel extract and the juice mediated NiCo_2O_4 nanostructures were compared
280 with those of pure NiCo_2O_4 nanostructures and bare nickel foam at various scan rates in 3.0M
281 KOH aqueous solution (Figure 4a-f). A redox peak is observed in all CV curves generated by
282 NiCo_2O_4 nanostructures, indicating that these nanostructures perform better than pseudo
283 capacitors in illustrating Faradic phenomena. Further, CV curves clearly indicate that Op-1
284 and Or- nanostructures have a higher area of curve than NiCo_2O_4 nanostructures prepared
285 with Op-2 and Or-2, indicating that these samples are capable of storing charge. In Figure 4,
286 CV curves of NiCo_2O_4 nanostructures were measured at different scan rates ranging from 10
287 to 110 mV/s, and their shape did not change with increasing scan rates. It can be concluded
288 from this that each sample of NiCo_2O_4 nanostructures exhibits significant stability as well as

289 rapid charge transfer kinetics. Furthermore, NiCo₂O₄ nanostructures prepared from orange
 290 peel extract and its fruit juice were compared with pure NiCo₂O₄ nanostructures and bare
 291 nickel foam at various current densities, including 1.5, 2, 2.5, 5 and 10 Ag⁻¹ (Figure 5). As
 292 prepared, NiCo₂O₄ nanostructures showed slightly different GCD curves from triangle shapes
 293 with well-oriented charge and discharge plateaus. Due to the increased Faradic activity at 1.5
 294 Ag⁻¹, the GCD curves and CV curves of Op-1 and Or-1 are highly suitable. To estimate the
 295 specific capacitance, equation [51] was used. In the presence of Op-1 and Op-2, the specific
 296 capacitance of (Cs) was determined to be 997.50, 780.00, 687.50, 637.50, 525.00, and
 297 862.50, 625.00, 537.50, 512.50, 500.00 Fg⁻¹ at various current densities of 1.5, 2, 2.5, 5, and
 298 10 Ag⁻¹, respectively. As a result, the specific capacitance of Or-1 and Or-2 was calculated at
 299 825.00, 730.00, 581.25, 562.50, 525.00 and 776.25, 695.00, 543.75, 525.00, 425.00 Fg⁻¹ at
 300 different current densities such as 1.5, 2, 2.5, 5, and 10 Ag⁻¹, respectively. For reference, the
 301 specific capacitances of pure NiCo₂O₄ nanostructures and bare nickel foam were also
 302 determined to be 533.42, 401.07, 374.33, 347.59, 320.86, and 461.23, 352.94, 320.86,
 303 294.12, 263.38 Fg⁻¹ at the same current densities as 1.5, 2, 2.5, 5, and 10 Ag⁻¹ as shown in
 304 (Figure 6). Calculations of specific capacitance (Cs) indicated Op-1 has 2-3-fold higher Cs
 305 than pure NiCo₂O₄ nanostructures, while bare nickel foam has 4-fold higher Cs.
 306 Nevertheless, Or-1 showed a slightly lower capacitance than Op-1, suggesting that the
 307 variation in supply of green reducing, capping, and stabilizing agents has a significant impact
 308 on NiCo₂O₄ nanostructures' electrochemical performance. Op-1 has excellent electrochemical
 309 kinetics and from the GCD curve distinctive pseudo capacitance properties are derived from
 310 the redox activity of bimetallic oxides as indicated by the plateau. Based on CV curves, this
 311 conclusion is well supported. Hydroxide ions (OH⁻) adsorb and desorb simultaneously in
 312 NiCo₂O₄ nanostructures, leading to pseudo capacitance functionality. Faradic transformations
 313 between Ni and Co (Co²⁺/Co³⁺, Ni²⁺/Ni³⁺, and Co³⁺/Co⁴⁺) are reversible, which have
 314 previously been generalized [52, 53].



317
 318

319 As a result of Cs' calculations, Op-1 achieved excellent performance due to controlled
 320 particle sizes, tuned surface properties, high electroactive site density, high rate of adsorption,
 321 large exposure to surface catalytic sites, nanoparticle compatibility with nickel foam during

322 low recapture sintering, and increased oxygen vacancies on the surface. These features are
323 desirable for high performance electrode materials for energy storage and conversion
324 systems, as demonstrated by using one mL of orange peel extract to reduce, cap, and stabilize
325 electrodes. Figure 6 shows the percentage specific capacitance retention, columbic efficiency,
326 energy, and power densities calculations. According to these results, OP-1 exhibited almost
327 100% specific capacitance retention, a columbic efficiency of 94% for 30000 cycle numbers,
328 and an energy density of 22.17 Wh/kg at 1.5Ag^{-1} as shown in (Figure 6).

329 The enhanced performance of NiCo_2O_4 nanostructures can be attributed to the multichannel
330 for the adsorption of hydroxide ions on nanoparticles deposited onto nickel foam, high
331 compatibility and adherence after low temperature sintering, a large surface area of the
332 electrode that is frequently interacted with electrolytic ions, and rapid charge transport at the
333 interface.

334 **3.3. Oxygen evolution reaction performance of as prepared various NiCo_2O_4** 335 **nanostructures**

336 Different NiCo_2O_4 nanostructures synthesized with orange peel extract and its fruit juice
337 were also investigated and compared with bare nickel foam and pure NiCo_2O_4 nanostructures
338 in 1.0M KOH solution. Figure 7a shows the results of measuring the first three CV cycles at a
339 slow scan rate of 5 mV/s followed by linear sweep voltammetry at 2 mV/s. CV was used
340 prior to LSV for electrochemically stabilizing electrodes in order to generate stable OER
341 signals. In order to maximize hydrogen production by electrochemical water splitting,
342 electrode materials with low onset potential, high overpotential, and high current density are
343 highly desirable [54, 55]. As a result, this study focused on the development of a high-
344 performance energy storage system as well as the same electrode material with high activity
345 for the OER water splitting reaction. Figure 7a shows the recorded LSV curves after iR
346 correction for the different NiCo_2O_4 nanostructures. LSV curves indicate that there is a
347 typical pre-oxidation peak between 1.25 and 1.4 V (versus RHE) for both $\text{Co}^{2+}/\text{Co}^{3+}$ or
348 $\text{Ni}^{2+}/\text{Ni}^{3+}$ in both materials, suggesting favorable conditions for efficient OER processes, as
349 such phenomena have already been well documented [56]. Compared to RHE, the OER onset
350 potentials of Op-1 and Op-2 were 1.31 V and 1.40 V, respectively. (Figure 7a) shows that the
351 OER onset potentials of Or-1 and Or-2 were 1.39 mV versus RHE and 1.38 mV versus RHE,
352 respectively [57, 58]. Nevertheless, NiCo_2O_4 nanostructures and bare nickel foam can have
353 onset potentials of 1.45 V and 1.46 V, respectively, as shown in (Figure 7a). Based on the

354 results of this analysis, Op-1 exhibited the lowest overpotential as compared to other samples,
 355 indicating that such electrode material has a high tendency to drive OER kinetics at low
 356 energy demands. It is possible to utilize this material to produce hydrogen quickly through
 357 electrochemical water splitting technology, which was highly emphasized in the previous
 358 study [59]. We also compared the OER performance with reported electrocatalysts based on
 359 Tafel analysis was performed on Op-1 and Op-2 to verify the OER rate and its kinetics
 360 aspects as shown in (Figure 7b). The Tafel slopes were 110 mVdec⁻¹ and 125 mVdec⁻¹,
 361 respectively. Tafel values were also 145 mVdec⁻¹ and 164 mVdec⁻¹ for Or-1 and Or-2,
 362 respectively. While the Tafel values of pure NiCo₂O₄ nanostructures and bare nickel foam
 363 were 170 mVdec⁻¹ and 204 mVdec⁻¹, respectively. It is confirmed from Tafel analysis that
 364 Op-1 can be utilized for practical water electrolysis as it has high efficiency towards OER.
 365 Previous studies [60, 61] found that the Tafel slope values matched the values calculated by
 366 Tafel. Under chemical equations [61], OER mechanism can be summarized as follows:



371
 372 A nonprecious electrocatalyst with significant stability is always desirable, and NiCo₂O₄
 373 nanostructures demonstrated negligible potential losses of less than 1%. In Figure 7c, the
 374 stability of the electrocatalyst after 45 hours of long-term use is demonstrated by the LSV
 375 curves, which demonstrate a high OER onset potential preservation and negligible loss in
 376 current density. Op-1's durability and stability could be used as potential electrode materials
 377 with excellent energy storage and conversion capabilities. It is essential to evaluate
 378 nonprecious electrocatalysts' durability before attempting to utilize electrochemical water
 379 splitting for hydrogen production. Hence, Or-1 was tested via chronoamperometry at 1.37 V
 380 versus RHE and 1.46 V versus RHE at constant potential for 45 h as shown in (Figure 7d,e).
 381 Both electrode materials have demonstrated significant durability to sustain 25 mA/cm²
 382 current density for 45 h without loss of current density.

383 Furthermore, electrochemical impedance spectroscopy (EIS) was used for determining the
 384 charge transfer at the interface to gain insight into the kinetics of electrode materials for
 385 electrochemical supercapacitors and OERs. The EIS was performed in 1.0M KOH aqueous

386 solution within the sweeping frequency range of 100 kHz to 0.1Hz with an amplitude of 10
387 mV and the onset potential of the OER. Previously, it has been demonstrated that the
388 diameter of the semicircle in the low frequency area of the Nyquist plot suggests fast
389 electrochemical reaction kinetics. In contrast, the lowest Rct value suggests long reaction
390 times [62, 63]. Figure 7f shows the Nyquist plots of Op-1, Op-2, Or-1 and Or-2 compared to
391 pure NiCo₂O₄ nanostructures and bare nickel foam. In Figure 7f, well-defined equivalent
392 circuits were obtained using Z-view software with circuit elements such as Rct, solution
393 resistance, and constant phase element (CPE). The Op-1 and Op-2 showed Rct values of 1.22
394 and 3.27 Ohms, respectively. Rct values were 3.17, and 4.89 Ohms for Or-1 and Or-2
395 respectively. NiCo₂O₄ nanostructures and bare nickel foam Rct values were respectively
396 22.01 and 25.43 Ohms. The Op-1 exhibited the lowest semicircle diameter compared to other
397 samples, indicating a rapid charge transfer rate between electrolyte and electrode material.

398 In order to quantify exposed catalytic sites towards an electrochemical reaction,
399 electrochemical active surface area (ECSA) is an essential contributing factor derived from
400 double layer capacitance (Cdl) [64-67]. (Figure 8a-f) shows the CV curves measured for
401 various samples with various NiCo₂O₄ nanostructures and bare nickel foam sweeping scan
402 rates used to calculate ECSA. The ECSA results for Op-1 and Op-2 were 39.32 and 33.15
403 μFcm^{-2} . The Or-1 and Or-2 possessed ECSA values 27.34 μFcm^{-2} , and 23.60 μFcm^{-2}
404 respectively. Pure NiCo₂O₄ nanostructures exhibited an ECSA value of 12.28 μFcm^{-2} , while
405 bare nickel foam exhibited an ECSA value of 8.38 μFcm^{-2} . As a result of ECSA calculations
406 as shown in (Figure 8g), it became apparent that ECSA's logical value exceeded Op-1
407 functionality. In NiCo₂O₄, fruit juice and orange peel extracts have induced abundant
408 electroactive sites, large surface oxygen vacancies, high amount of Co (III) ions on the
409 surface, high exposure of surface area of nanoparticles to the electrolyte, multiple charge
410 transfer channels, enhanced compatibility of particles with the nickel foam, favorable redox
411 processes, and efficient adsorption of hydroxide ions from the electrolyte, resulting in
412 improved electrochemical activity. Based on SEM, XRD, XPS, HRTEM, EIS, and ECSA
413 analysis, positive results have been identified for enhanced electrochemical charge storage
414 and OER applications.

415 **4. Conclusions**

416 During the hydrothermal synthesis of NiCo₂O₄ nanostructures, orange peel extract and fruit
417 juice can provide green reducing, capping, and stabilizing agents. These agents can be further

418 enhanced by thermal annealing in air at 500 ° C after thermal reduction. After the NiCo₂O₄
419 nanostructures had been prepared, they were fabricated onto nickel foam by dip coating and
420 low-temperature sintering to ensure a high degree of compatibility. The morphology, crystal
421 properties, oxidation states of the metal, and surface vacancies were examined using SEM,
422 XRD, HRTEM, and XPS techniques. A structural and functional analysis of Op-1 revealed an
423 outstanding performance with a 997.50 Fg⁻¹ specific capacitance and a capacitance retention
424 rate of nearly 100% after 30000 cycles of GCD at 1.5 Ag⁻¹. Additionally, OER was
425 accomplished at markedly low (120 mV) overpotential at 20 mA/cm² with a 110 mVdec⁻¹
426 Tafel slope and more than 45 h of stability. It has been demonstrated that several factors
427 contribute to the superior performance of NiCo₂O₄ nanostructures prepared using orange peel
428 extract. The high concentration of electroactive sites, the large surface area, the compatibility
429 of nanoparticles with nickel foam, the rapid charge transfer rate at the interface, the
430 abundance of oxygen vacancies on the surface, and the enhanced electrical conductivity are
431 all factors contributing to this performance.

432 **Acknowledgment**

433 The authors would like to gratefully acknowledge the Higher Education Commission
434 Pakistan for partial support under the project NRPU/8350. We also extend our sincere
435 appreciation to the Researchers Supporting Project Number (RSP2023R66) at King Saud
436 University, Riyadh, Saudi Arabia. Brigitte Vigolo and Mélanie Emo would like to thank the
437 platform “Microscopies, Microprobes and Metallography (3 M)” (Institut Jean Lamour, IJL,
438 Nancy, France) for access to TEM and SEM facilities. Authors would also like to
439 acknowledge partial funding of the Ajman University, Grant ID: DRG ref. 2023-IRG-HBS-2
440 (RESHUSC-001). This publication is part of the R&D project PID2021-126235OB-C32
441 funded by MCIN/AEI/10.13039/501100011033/ and FEDER funds.

442 **Conflict of Interest**

443 Authors declare no competing interests in the resented research work.

444 **Data Availability Statements**

445 Data sets generated during the current study are available from the corresponding author on
446 reasonable request.

447

449 **References**

- 450 1. Y. Zhao, M. Liu, X. Deng, L. Miao, P.K. Tripathi, X. Ma, L. Gan, Nitrogen-
451 functionalized microporous carbon nanoparticles for high performance supercapacitor
452 electrode. *Electrochimica Acta* 153 (2015) 448-455.
- 453 2. M. Chen, J. Liu, D. Chao, J. Wang, J. Yin, J. Lin, Z.X. Shen, Porous α -Fe₂O₃
454 nanorods supported on carbon nanotubes-graphene foam as superior anode for lithium
455 ion batteries. *Nano Energy* 9 (2014) 364-372.
- 456 3. A. Bashir, S. Shukla, R. Bashir, R. Patidar, A. Bruno, D. Gupta, Z. Akhter, Low
457 temperature, solution processed spinel NiCo₂O₄ nanoparticles as efficient hole
458 transporting material for mesoscopic nip perovskite solar cells. *Solar Energy* 196
459 (2020) 367-378.
- 460 4. M. Kuang, Z.Q. Wen, X.L. Guo, S.M. Zhang, Y.X. Zhang, Engineering firecracker-
461 like beta-manganese dioxides@ spinel nickel cobaltates nanostructures for high-
462 performance supercapacitors. *Journal of Power Sources* 270 (2014) 426-433.
- 463 5. M.J. Pang, S. Jiang, G.H. Long, Y. Ji, W. Han, B. Wang, G.D. Wei, Mesoporous NiCo
464 ₂ O ₄ nanospheres with a high specific surface area as electrode materials for high-
465 performance supercapacitors. *RSC advances* 6 (2016) 67839-67848.
- 466 6. H. Zhu, D. Zhang, H.S. Athab, B. Wu, Y. Gu, PV isolated three-port converter and
467 energy-balancing control method for PV-battery power supply applications. *IEEE*
468 *Transactions on Industrial Electronics* 62 (2014) 3595-3606.
- 469 7. Y. Zou, C. Cai, C. Xiang, P. Huang, H. Chu, Z. She, H.B. Kraatz, Simple synthesis of
470 core-shell structure of Co-Co₃O₄@ carbon-nanotube-incorporated nitrogen-doped
471 carbon for high-performance supercapacitor. *Electrochimica Acta* 261 (2018) 537-
472 547.
- 473 8. W. Yan, J. Bi, W. Wang, Z. Xing, R. Liu, X. Hao, M. Leng, Hierarchical MnO₂@
474 NiCo₂O₄@ Ti₃SiC₂/carbon cloth core-shell structure with superior electrochemical
475 performance for all solid-state supercapacitors. *Ceramics International* 47 (2021) 292-
476 300.
- 477 9. T. Zhao, C. Liu, F. Yi, W. Deng, A. Gao, D. Shu, L. Zheng, Hollow N-doped carbon@
478 O-vacancies NiCo₂O₄ nanocages with a built-in electric field as high-performance
479 cathodes for hybrid supercapacitor. *Electrochimica Acta* 364 (2020) 137260.
- 480 10. W. Wang, M.T. Winkler, O. Gunawan, T. Gokmen, T.K. Todorov, Y. Zhu, D.B. Mitzi,
481 Device characteristics of CZTSSe thin- film solar cells with 12.6%
482 efficiency. *Advanced energy materials* 4 (2014) 1301465.
- 483 11. P. Bhojane, S. Sen, P.M. Shirage, Enhanced electrochemical performance of
484 mesoporous NiCo₂O₄ as an excellent supercapacitive alternative energy storage
485 material. *Applied surface science* 377 (2016) 376-384.
- 486 12. J.R. Miller, P. Simon, Electrochemical capacitors for energy management. *Science*
487 321 (2018) 651-652.
- 488 13. G. Wang, L. Zhang, J. Zhang, A review of electrode materials for electrochemical
489 supercapacitors. *Chemical Society Reviews* 41 (2012) 797-828.
- 490 14. Y. Shi, Y. Zhao, K. Wang, X. Shi, Y. Wang, H. Huang, F. Shao, Cleavage of
491 GSDMD by inflammatory caspases determines pyroptotic cell death. *Nature* 526
492 (2015) 660-665.
- 493 15. L. Zhou, Y. Tan, J. Wang, W. Xu, Y. Yuan, W. Cai, J. Zhu, 3D self-assembly of
494 aluminium nanoparticles for plasmon-enhanced solar desalination. *Nature Photonics*
495 10 (2016) 393-398.

- 496 16. W. Liu, Y. Chen, Y. Wang, Q. Zhao, L. Chen, W. Wei, J. Ma, Influence of anion
497 substitution on 3D-architected Ni-Co-A (A= H, O, P) as efficient cathode materials
498 towards rechargeable Zn-based battery. *Energy Storage Materials* 37 (2021) 336-344.
- 499 17. Y. Zeng, Z. Lai, Y. Han, H. Zhang, S. Xie, X. Lu, Oxygen- vacancy and surface
500 modulation of ultrathin nickel cobaltite nanosheets as a high- energy cathode for
501 advanced Zn- ion batteries. *Advanced Materials* 30 (2018) 1802396.
- 502 18. J. Bao, X. Zhang, B. Fan, J. Zhang, M. Zhou, W. Yang, Y. Xie, Ultrathin
503 spinel- structured nanosheets rich in oxygen deficiencies for enhanced
504 electrocatalytic water oxidation. *Angewandte Chemie* 127 (2015) 7507-7512.
- 505 19. T.Y. Wei, C.H. Chen, H.C. Chien, S.Y. Lu, C.C. Hu, A cost- effective supercapacitor
506 material of ultrahigh specific capacitances: spinel nickel cobaltite aerogels from an
507 epoxide- driven sol-gel process. *Advanced materials* 22 (2010) 347-351.
- 508 20. Y. Li, X. Han, T. Yi, Y. He, X. Li, Review and prospect of NiCo₂O₄-based
509 composite materials for supercapacitor electrodes. *Journal of energy chemistry* 31
510 (2019) 54-78.
- 511 21. Z. Luo, D. Shu, F. Yi, J. Ling, M. Wang, C. Huang, A. Gao, Urchin-like NiCo₂O₄
512 hollow microspheres with oxygen vacancies synthesized by self-template for
513 supercapacitor. *New Journal of Chemistry* 45 (2020) 22748-22757.
- 514 22. X. Chen, L. Song, M. Zeng, L. Tong, C. Zhang, K. Xie, Y. Wang, Regulation of
515 morphology and electronic configuration of NiCo₂O₄ by aluminum doping for high
516 performance supercapacitors. *Journal of Colloid and Interface Science* 610 (2020) 70-
517 79.
- 518 23. O. Stoian, C.I. Covaliu, G. Paraschiv, G.A. Catrina, M. Niță-Lazăr, E. Matei, P. Tudor,
519 Magnetite oxide nanomaterial used for lead ions removal from industrial
520 wastewater. *Materials* 14 (2021) 2831.
- 521 24. P. Kaur, R. Thakur, J.S. Duhan, A. Chaudhury, Management of wilt disease of
522 chickpea in vivo by silver nanoparticles biosynthesized by rhizospheric microflora of
523 chickpea (*Cicer arietinum*). *Journal of Chemical Technology & Biotechnology* 93
524 (2018) 3233-3243.
- 525 25. L.K. Ruddaraju, S.V.N. Pammi, G. Sankar Guntuku, V.S. Padavala, V.R. Kolapalli, A
526 review on anti-bacterials to combat resistance: From ancient era of plants and metals
527 to present and future perspectives of green nano technological combinations. *Asian*
528 *Journal of Pharmaceutical Sciences* 15 (2020) 42-59.
- 529 26. A. Thapa, Sustainable Development Goal-6 (clean water and sanitation) Status and
530 Challenges in Nepal. *Journey for Sustainable Development and Peace Journal* 1
531 (2023) 21-35.
- 532 27. Z.H. Jaffari, A. Abbas, S.M. Lam, S. Park, K. Chon, E.S. Kim, K.H. Cho, Machine
533 learning approaches to predict the photocatalytic performance of bismuth ferrite-
534 based materials in the removal of malachite green. *Journal of Hazardous*
535 *Materials* 442 (2023) 130031.
- 536 28. K.M. Abualnaja, A.E. Alprol, M.A. Abu-Saied, M. Ashour, A.T. Mansour, Removing
537 of anionic dye from aqueous solutions by adsorption using of multiwalled carbon
538 nanotubes and poly (Acrylonitrile-styrene) impregnated with activated
539 carbon. *Sustainability* 13 (2021) 7077.
- 540 29. M.M. Mabrouk, M. Ashour, A. Labena, M.A. Zaki, A.F. Abdelhamid, M.S. Gewaily,
541 H.F. Ayoub, Nanoparticles of *Arthrospira platensis* improves growth, antioxidative
542 and immunological responses of Nile tilapia (*Oreochromis niloticus*) and its resistance
543 to *Aeromonas hydrophila*. *Aquaculture Research* 53 (2022) 125-135.

- 544 30. A.T. Mansour, A.E. Alprol, K.M. Abualnaja, H.S. El-Beltagi, K.M. Ramadan, M.
545 Ashour, The Using of Nanoparticles of Microalgae in Remediation of Toxic Dye from
546 Industrial Wastewater: Kinetic and Isotherm Studies. *Materials* 15 (2022) 3922.
- 547 31. A.T. Mansour, A.E. Alprol, M. Ashour, K.M. Ramadan, A.H Alhajji, K.M. Abualnaja,
548 Do Red Seaweed Nanoparticles Enhance Bioremediation Capacity of Toxic Dyes
549 from Aqueous Solution?. *Gels* 8 (2022) 310.
- 550 32. A.T. Mansour, A.E. Alprol, M. Khedawy, K.M. Abualnaja, T.A. Shalaby, G. Rayan,
551 M. Ashour, Green synthesis of zinc oxide nanoparticles using red seaweed for the
552 elimination of organic toxic dye from an aqueous solution. *Materials* 15 (2022) 5169.
- 553 33. Z.Z. Sharawy, M. Ashour, A. Labena, A.S. Alsaqafi, A.T. Mansour, E.M. Abbas,
554 Effects of dietary *Arthrospira platensis* nanoparticles on growth performance, feed
555 utilization, and growth-related gene expression of Pacific white shrimp, *Litopenaeus*
556 *vannamei*. *Aquaculture* 551 (2022) 737905.
- 557 34. B. Kumar, K. Smita, L. Cumbal, A. Debut, Y. Angulo, Biofabrication of copper oxide
558 nanoparticles using Andean blackberry (*Rubus glaucus* Benth.) fruit and leaf. *Journal*
559 *of Saudi Chemical Society* 21 (2017) S475-S480.
- 560 35. A.E. Alprol, A.T. Mansour, H.S. El-Beltagi, M. Ashour, Algal Extracts for Green
561 Synthesis of Zinc Oxide Nanoparticles: Promising Approach for Algae
562 Bioremediation. *Materials* 16 (2023) 2819.
- 563 36. S. Kumar, A. Tahira, M. Emo, B. Vigolo, A. Infantes-Molin, A.M. Alotaibi, Z.H.
564 Ibupoto, Grapefruit juice containing rich hydroxyl and oxygenated groups capable of
565 transforming 1D structure of NiCo_2O_4 into 0D with excessive surface vacancies for
566 promising energy conversion and storage applications. *Journal of Energy Storage* 68
567 (2023) 107708.
- 568 37. S. Kumar, A. Tahira, A.L. Bhatti, M.A. Bhatti, R.H. Mari, N.M. Shaikh, Z.H. Ibupoto,
569 Transforming NiCo_2O_4 nanorods into nanoparticles using citrus lemon juice
570 enhancing electrochemical properties for asymmetric supercapacitor and water
571 oxidation. *RSC advances* 13 (2023) 18614-18626.
- 572 38. USDA (United States Department of Agriculture) Citrus: World Markets and
573 Trade. (<http://www.fas.usda.gov/data/citrus-world-markets-and-trade>) 2014.
- 574 39. F.R. Marín, C. Soler-Rivas, O. Benavente-García, J. Castillo, J.A. Pérez-Alvarez, By-
575 products from different citrus processes as a source of customized functional
576 fibres. *Food chemistry* 100 (2007) 736-741.
- 577 40. F. Morton, Julia (1987). "Mandarin orange; In: *Fruits of Warm Climates*, . New Crop
578 Resource Online Program. Center for New Crops and Plant Products, Purdue
579 University. Retrieved 8 March (2019) 142-145.
- 580 41. L. Wang, F. He, Y. Huang, J. He, S. Yang, J. Zeng, Q. Xu, Genome of wild mandarin
581 and domestication history of mandarin. *Molecular plant*. 11 (2018) 1024-1037.
- 582 42. Mandarin orange production in 2020 (includes tangerines, clementines, and
583 satsumas)". FAOSTAT, United Nations Corporate Statistical Database. 2022.
584 Retrieved 11 September 2022.
- 585 43. M. Láinez, H.A. Ruiz, A.A. Castro-Luna, S. Martínez-Hernández, Release of simple
586 sugars from lignocellulosic biomass of *Agave salmiana* leaves subject to sequential
587 pretreatment and enzymatic saccharification. *Biomass and bioenergy* 118 (2018) 133-
588 140.
- 589 44. <https://bio-norm.com/product/orange-peel-extract/>
- 590 45. A.L. Bhatti, A. Tahira, S. Kumar, Z.A. Ujjan, M.A. Bhatti, S. Kumar, Z.H. Ibupoto,
591 Facile synthesis of efficient Co_3O_4 nanostructures using the milky sap of *Calotropis*

- 592 procera for oxygen evolution reactions and supercapacitor applications. RSC
593 advances 13 (2023) 17710-17726.
- 594 46. A.J. Laghari, U. Aftab, A.A. Shah, M.Y. Solangi, M.I. Abro, S.I. Al-Saedi, Z.H.
595 Ibhupoto, Surface modification of Co₃O₄ nanostructures using wide range of natural
596 compounds from rotten apple juice for the efficient oxygen evolution
597 reaction. International Journal of Hydrogen Energy 48 (2023) 15447-15459.
- 598 47. Bhatti, A. L.; Tahira, A.; Gradone, A.; Mazzaro, R.; Morandi, V.; Abro, M. I.; Ibupoto,
599 Z. H. Nanostructured Co₃O₄ electrocatalyst for OER: the role of organic
600 polyelectrolytes as soft templates. Electrochimica Acta 2021, 398, 139338.
- 601 48. U. Aftab, A. Tahira, R. Mazzaro, M.I. Abro, M.M. Baloch, M. Willander, Z.H.
602 Ibupoto, The chemically reduced CuO–Co₃O₄ composite as a highly efficient
603 electrocatalyst for oxygen evolution reaction in alkaline media. Catalysis Science &
604 Technology 9 (2019) 6274-6284.
- 605 49. Y.T. Lu, Y.J. Chien, C.F. Liu, T.H. You, C.C. Hu, Active site-engineered bifunctional
606 electrocatalysts of ternary spinel oxides, M_{0.1}Ni_{0.9}Co₂O₄ (M: Mn, Fe, Cu, Zn)
607 for the air electrode of rechargeable zinc–air batteries. Journal of Materials Chemistry
608 A. 5 (2017) 21016-21026.
- 609 50. Y.L. Tong, L. Xing, M.Z. Dai, X. Wu, Hybrid Co₃O₄@ Co₉S₈ electrocatalysts for
610 oxygen evolution reaction. Frontiers in Materials 6 (2019) 233.
- 611 51. D. Lei, X.D. Li, M.K. Seo, M.S. Khil, H.Y. Kim, B.S. Kim, NiCo₂O₄ nanostructure-
612 decorated PAN/lignin based carbon nanofiber electrodes with excellent cyclability for
613 flexible hybrid supercapacitors. Polymer 132 (2017) 31-40.
- 614 52. E. Jokar, A.I. Zad, S. Shahrokhian, Synthesis and characterization of NiCo₂O₄
615 nanorods for preparation of supercapacitor electrodes, J Solid State Electrochem 19
616 (2015) 269–274.
- 617 53. X. Wang, W.S. Liu, X. Lu, P.S. Lee, Dodecyl sulfate-induced fast faradic process in
618 nickel cobalt oxide–reduced graphite oxide composite material and its application for
619 asymmetric supercapacitor device. Journal of Materials Chemistry 22 (2012) 23114-
620 23119.
- 621 54. S. Peng, L. Li, H.B. Wu, S. Madhavi, X.W. Lou, Controlled growth of NiMoO₄
622 nanosheet and nanorod arrays on various conductive substrates as advanced electrodes
623 for asymmetric supercapacitors. Advanced Energy Materials 5 (2015) 1401172.
- 624 55. Y. Ma, X. Dai, M. Liu, J. Yong, H. Qiao, A. Jin, X. Zhang, Strongly coupled FeNi
625 alloys/NiFe₂O₄@ carbonitride layers-assembled microboxes for enhanced oxygen
626 evolution reaction. ACS applied materials & interfaces 8 (2016) 34396-34404.
- 627 56. J. Zhu, Z. Liu, M. Zhai, Y. Ni, Ni_{1-x}Co_xSe nanostructures deposited on nickel foam
628 by a facile potentiostatic route for enhanced OER performance. Journal of Physics
629 and Chemistry of Solids 148 (2021) 109658.
- 630 57. A. Fauzi, S. Geng, F. Tian, Y. Liu, H. Li, Y. Yu, J. Li, W. Yang, NiFe-LDH@ Ni₃S₂
631 supported on nickel foam as highly active electrocatalysts for oxygen evolution
632 reaction. International Journal of Hydrogen Energy. 48 (2023) 1370-9.
- 633 58. K. Cysewska, M.K. Rybarczyk, G. Cempura, J. Karczewski, M. Łapiński, P. Jasinski,
634 S. Molin, The Influence of the Electrodeposition Parameters on the Properties of Mn-
635 Co-Based Nanofilms as Anode Materials for Alkaline Electrolysers. Materials. 13
636 (2020) 2662.
- 637 59. Z. Dai, X. Du, X. Zhang, Controlled synthesis of NiCo₂O₄@ Ni-MOF on Ni foam as
638 efficient electrocatalyst for urea oxidation reaction and oxygen evolution
639 reaction. International Journal of Hydrogen Energy 47 (2022) 17252-17262.

640 60. K. Xiang, D. Wu, Y. Fan, W. You, D. Zhang, J.L. Luo, X.Z. Fu, Enhancing
641 bifunctional electrodes of oxygen vacancy abundant ZnCo₂O₄ nanosheets for
642 supercapacitor and oxygen evolution. *Chemical Engineering Journal* 425 (2021)
643 130583.

644 61. L. Zhang, H. Yuan, X. Li, Y. Wang, Hydrothermal Synthesis of NiCo₂O₄@ NiCo₂O₄
645 Core-Shell Nanostructures Anchored on Ni Foam for Efficient Oxygen Evolution
646 Reactions Catalysts. *Coatings* 12 (2022) 1240.

647 62. H. Feng, S. Gao, J. Shi, L. Zhang, Z. Peng, S. Cao, Construction of 3D hierarchical
648 porous NiCo₂O₄/graphene hydrogel/Ni foam electrode for high-performance
649 supercapacitor. *Electrochimica Acta* 299 (2019) 116-124.

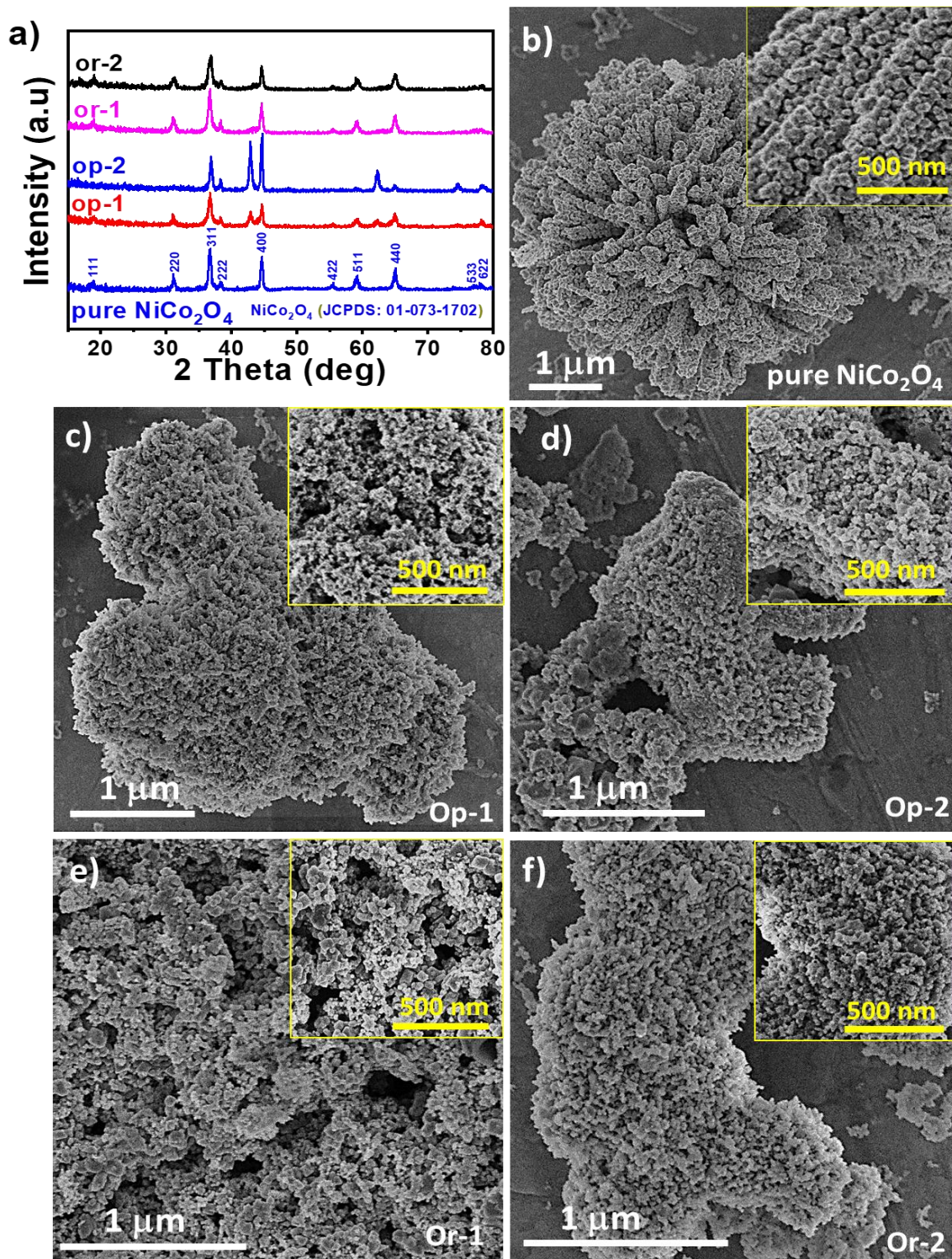
650 63. X. Long, J. Li, S. Xiao, K. Yan, Z. Wang, H. Chen, S. Yang, A strongly coupled
651 graphene and FeNi double hydroxide hybrid as an excellent electrocatalyst for the
652 oxygen evolution reaction. *Angewandte Chemie International Edition* 53 (2014) 7584-
653 7588.

654 64. Y. Huang, L.W. Jiang, X.L. Liu, T. Tan, H. Liu, J.J. Wang, Precisely engineering the
655 electronic structure of active sites boosts the activity of iron-nickel selenide on nickel
656 foam for highly efficient and stable overall water splitting. *Applied Catalysis B:
657 Environmental* 299 (2021) 120678.

658 65. H. Feng, S. Gao, J. Shi, L. Zhang, Z. Peng, S. Cao, Construction of 3D hierarchical
659 porous NiCo₂O₄/graphene hydrogel/Ni foam electrode for high-performance
660 supercapacitor. *Electrochimica Acta*. 299 (2019) 116-124.

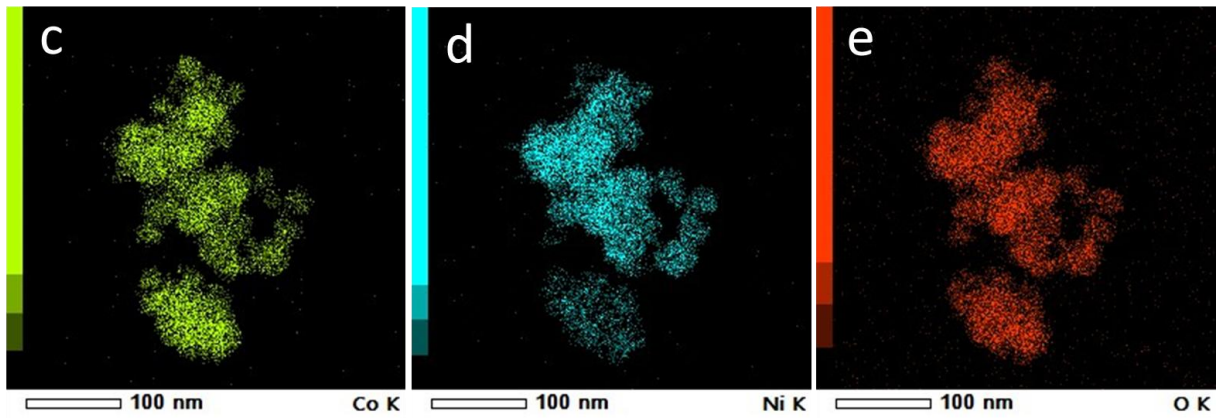
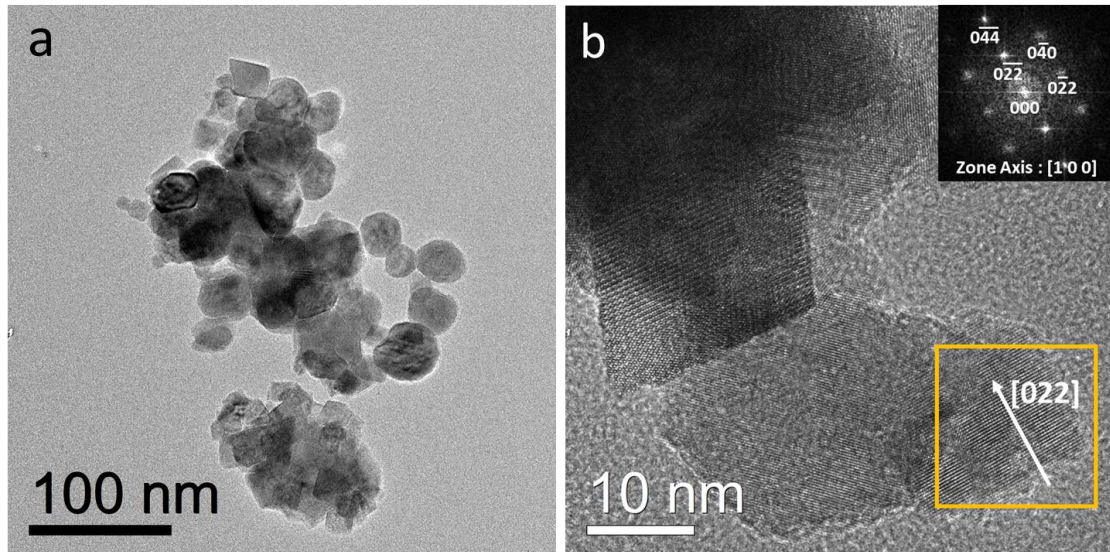
661 66. L. Zhang, H. Li, K. Li, L. Li, J. Wei, L. Feng, Q. Fu, Morphology-controlled
662 fabrication of Co₃O₄ nanostructures and their comparative catalytic activity for
663 oxygen evolution reaction. *Journal of Alloys and Compounds*. 680 (2016) 146-154.

664 67. S. Jiang, K. Ithisuphalap, X. Zeng, G. Wu, H. Yang, 3D porous cellular
665 NiCoO₂/graphene network as a durable bifunctional electrocatalyst for oxygen
666 evolution and reduction reactions. *Journal of Power Sources*, 399 (2018) 66-75.
667
668
669
670
671
672
673
674
675
676
677
678
679
680
681
682
683
684
685
686
687
688



690

691 **Fig. 1** a) XRD patterns of pure NiCo_2O_4 nanostructures , Op-1, Op-2, Or-1, and Or-2) and
 692 SEM images of NiCo_2O_4 nanostructures synthesized without and with orange based
 693 additives: b) without any orange based additives, c) and d) Op-1 and Op-2), e) and f) Or-1
 694 and Or-2). Inserts are SEM images of higher magnification.

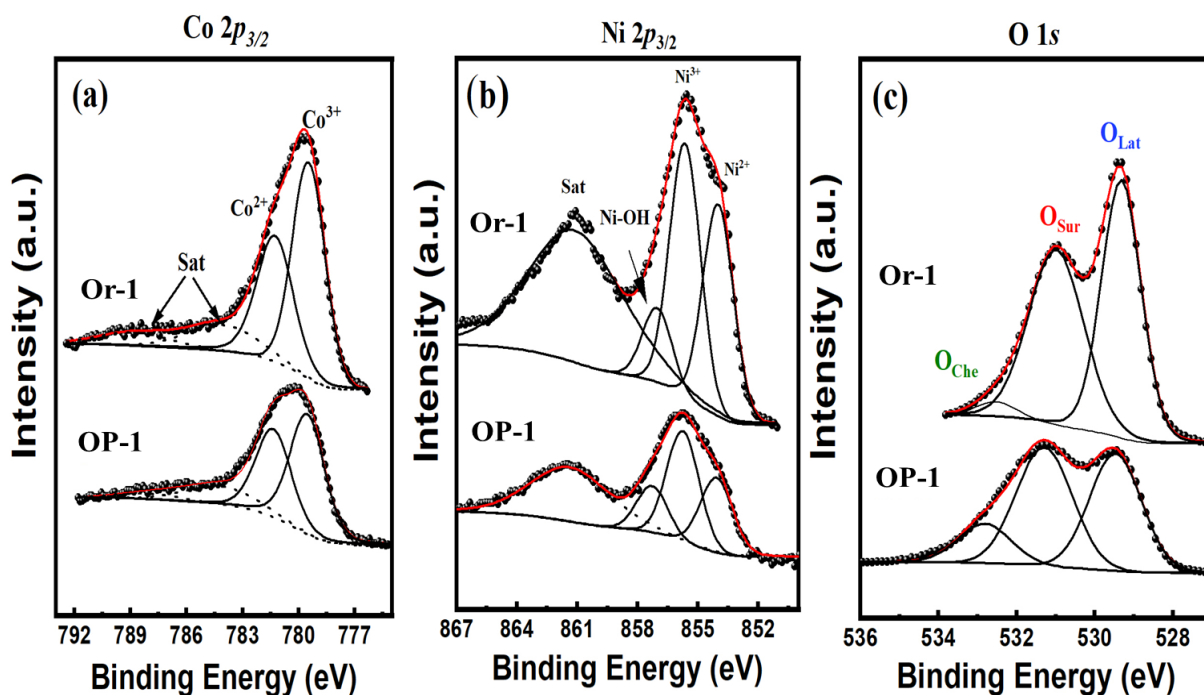


695

696 Fig. 2. (a) TEM image and (b) HRTEM micrograph with corresponding Fast Fourier Transform (FFT)
 697 of one nanoparticle (yellow square) (in insert) of Op-1t and corresponding X-maps of cobalt (d),
 698 nickel (e) and oxygen (f).

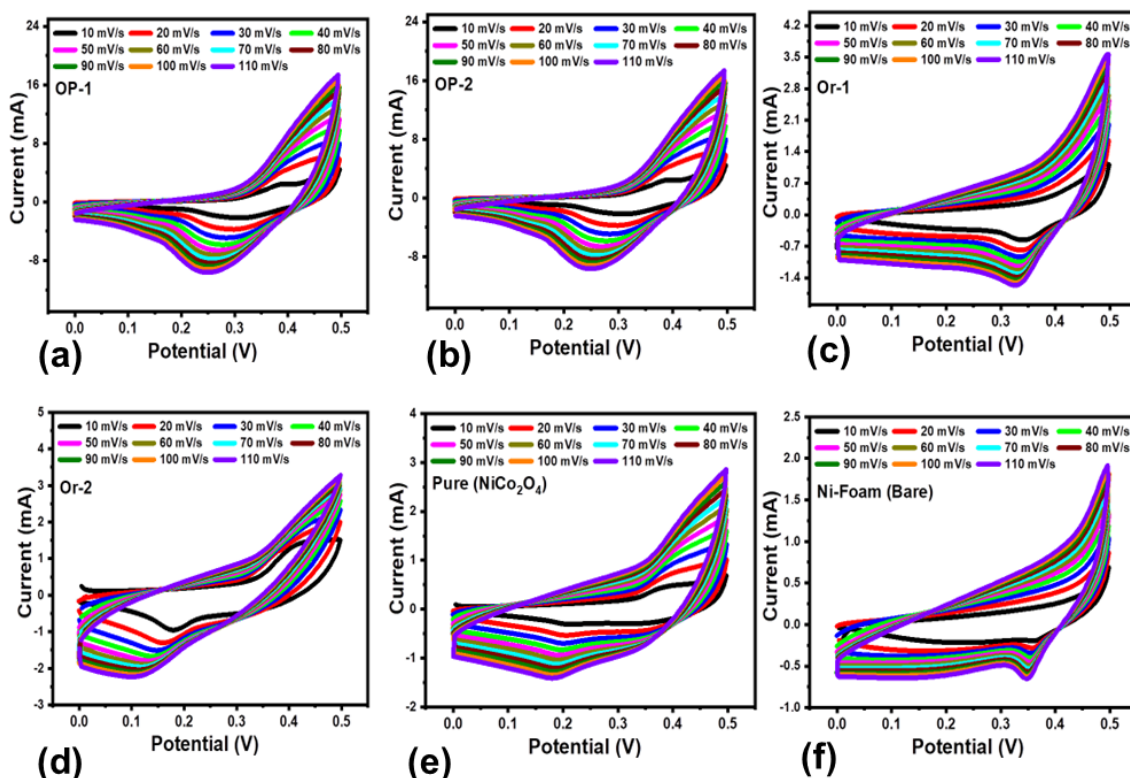
699

700



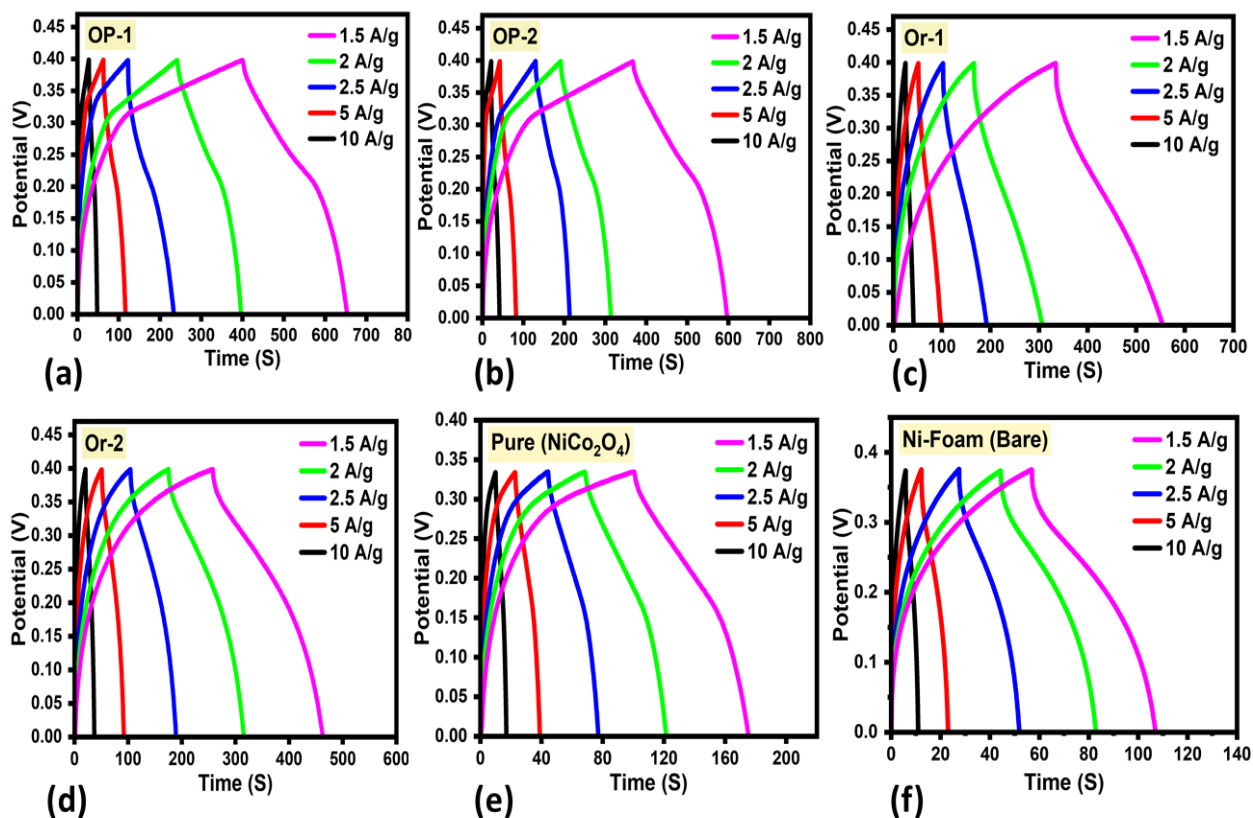
701

702 **Fig. 3.** X-ray core level spectra of different NiCo₂O₄ nanostructures prepared with 1 mL orange peel
 703 extract (Op-1) and its fruit juice (Or-1), (a) Co 2p_{3/2}, (b) Ni 2p_{3/2} (c) O 1s.



704

705 **Fig. 4.** CV curves of NiCo₂O₄ nanostructures synthesized with 1 mL and 2 mL of orange peel
 706 extract (Op-1, Op-2) and its fruit juice (Or-1, Or-2) at different scan rates in 3.0M KOH aqueous solution,
 707 (e-f) CV curves of pure NiCo₂O₄ nanostructures and bare nickel foam respectively at various scan
 708 rates in 3.0 M KOH aqueous solution.

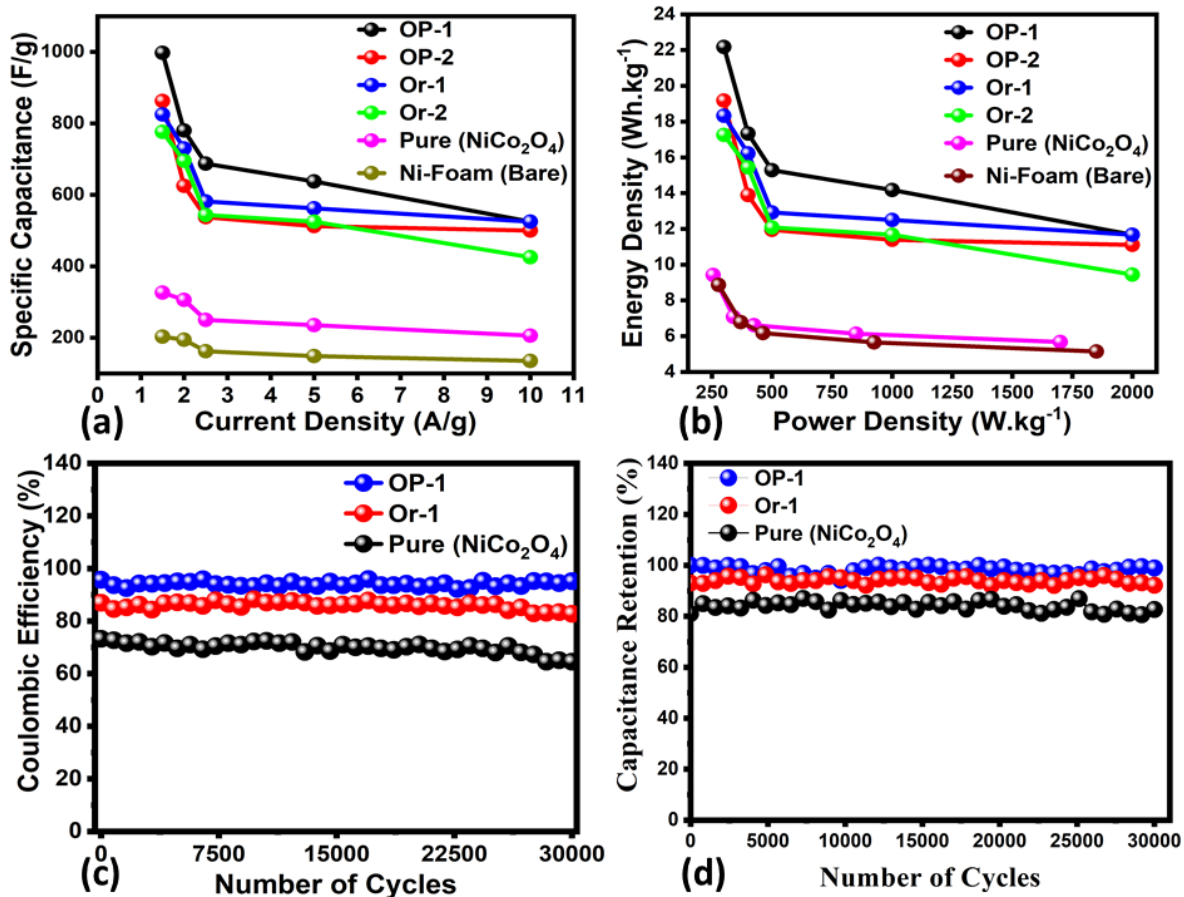


709

710 **Fig. 5.** (a-d) GCD curves of NiCo₂O₄ nanostructures prepared with 1 mL and 2 mL of orange peel
 711 extract (Op-1, Op-2) and its fruit juice (Or-1, Or-2) at different current densities in 3.0M KOH
 712 aqueous solution, (e-f) GCD curves of pure NiCo₂O₄ nanostructures and bare nickel foam respectively
 713 at various current densities in 3.0 M KOH aqueous solution.

714

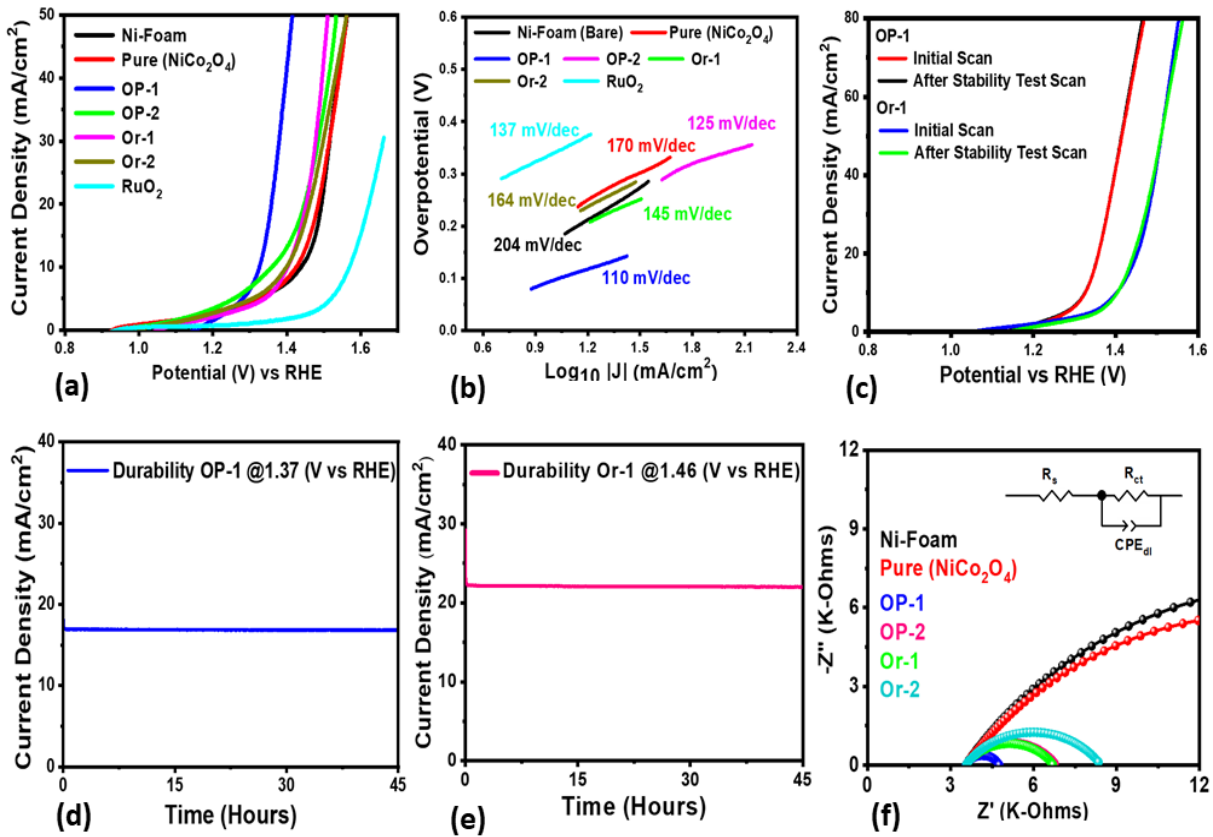
715



716

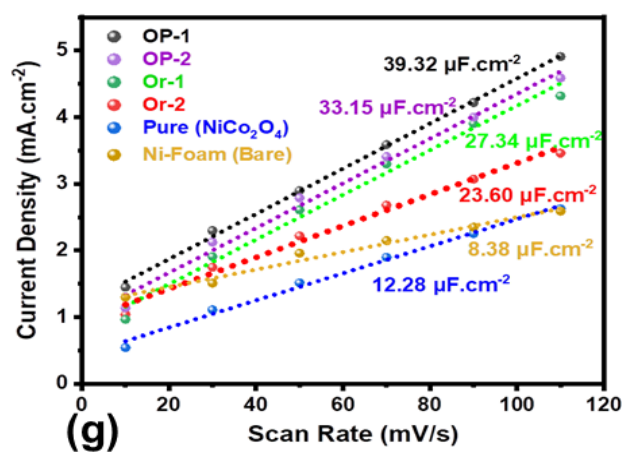
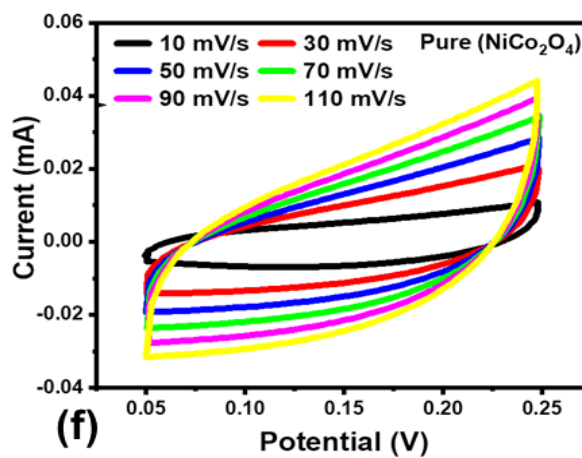
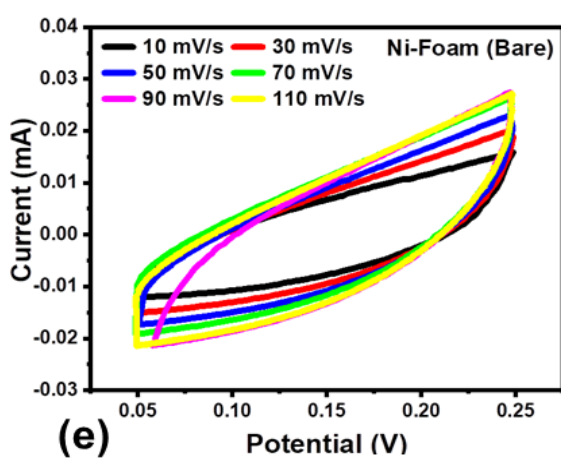
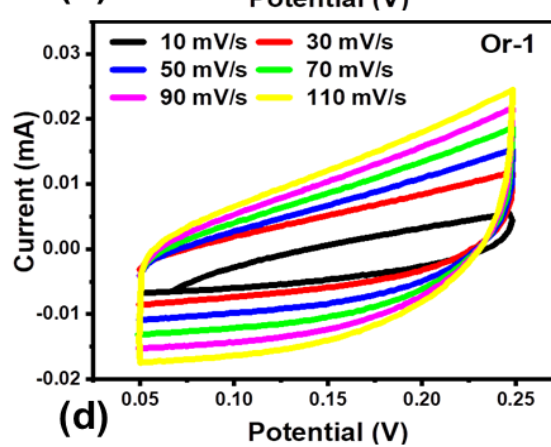
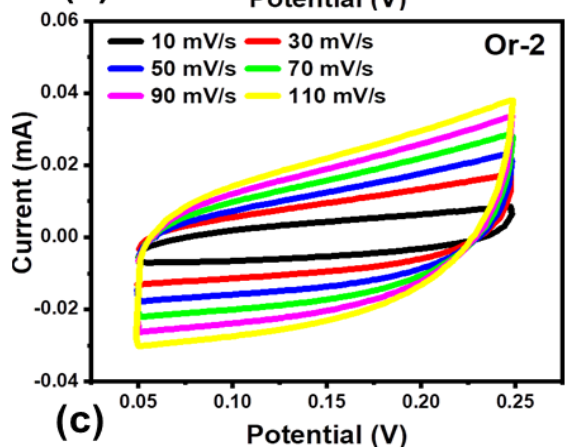
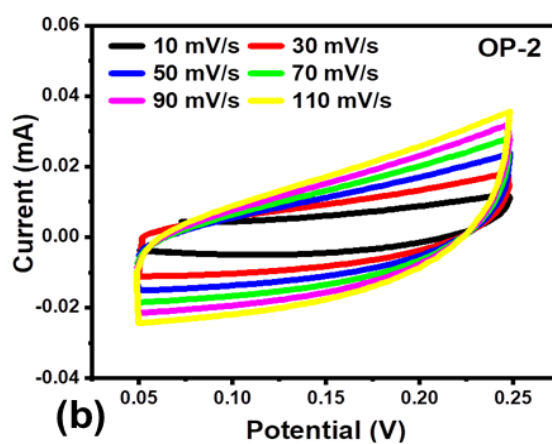
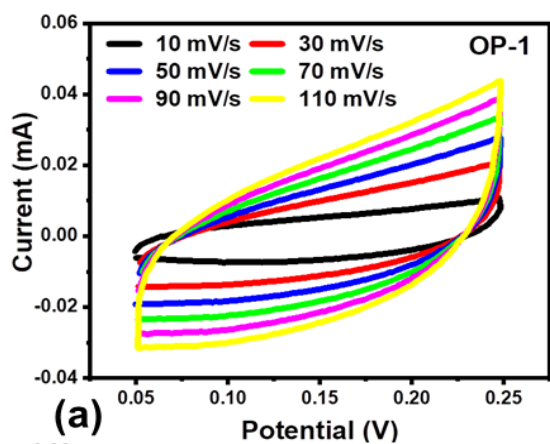
717

718 **Fig. 6.** (a) Calculated specific capacitance from GCD curves for different NiCo_2O_4 nanostructures
 719 prepared with 1 mL and 2 mL of orange peel extract (Op-1, Op-2) and its fruit juice (Or-1, Or-2),
 720 pure NiCo_2O_4 nanostructures and bare nickel foam respectively in 3.0 M KOH aqueous solution, (b)
 721 corresponding energy density of different NiCo_2O_4 nanostructures from GCD curves, (c) columbic
 722 efficiency of different NiCo_2O_4 nanostructures prepared with 1 mL orange peel extract (Op-1) and
 723 its fruit juice (Or-1), pure NiCo_2O_4 nanostructures rom 30000 GCD repeatable cycles in 3.0 M KOH,
 724 (d) Corresponding percentage retention specific capacitance of different NiCo_2O_4 nanostructures
 725 prepared with 1 mL orange peel extract (Op-1) and its fruit juice (Or-1), pure NiCo_2O_4
 726 nanostructures rom 30000 GCD repeatable cycles in 3.0 M KOH for the illustration of cycling
 727 stability.



728

729 **Fig. 7.** (a) LSV curves at 2 mV/s for different NiCo_2O_4 nanostructures prepared with 1 mL and 2 mL
 730 of orange peel extract (Op-1, Op-2) and its fruit juice (Or-1, Or-2), RuO_2 , pure NiCo_2O_4
 731 nanostructures and bare nickel foam respectively in 1.0 M KOH aqueous solution (b) Related Tafel
 732 analysis, (c) stability of NiCo_2O_4 nanostructures prepared with 1 mL of orange peel extract (Op-1)
 733 and its fruit juice (Or-1) before and after durability tests, (d,e) durability of NiCo_2O_4 nanostructures
 734 prepared with 1 mL of orange peel extract (Op-1) and its fruit juice (Or-1) for 45 h using
 735 chronoamperometry at 1.37 V versus REHE and 1.46 V versus RHE respectively (f) EIS Nyquist
 736 plots of different NiCo_2O_4 nanostructures prepared with 1 mL and 2 mL of orange peel extract (Op-
 737 1, Op-2) and its fruit juice (Or-1, Or-2), pure NiCo_2O_4 nanostructures and bare nickel foam
 738 respectively using frequency window of f 100 kHz to 0.1 Hz at an amplitude of 10 mV and OER
 739 onset potential, inset shows the fitted equivalent circuit in 1.0M KOH aqueous solution.



740

741

742 **Fig. 8.** (a-f) CV curves of different NiCo_2O_4 nanostructures prepared with 1 mL and 2 mL of orange
 743 peel extract (Op-1, Op-2) and its fruit juice (Or-1, Or-2), pure NiCo_2O_4 nanostructures and bare
 744 nickel foam respectively in 1.0 M KOH aqueous solution at various scan rates in 1.0M KOH, (g)
 745 Corresponding calculated ECSA from non-Faradic part presented CV curves of different NiCo_2O_4
 746 nanostructures.

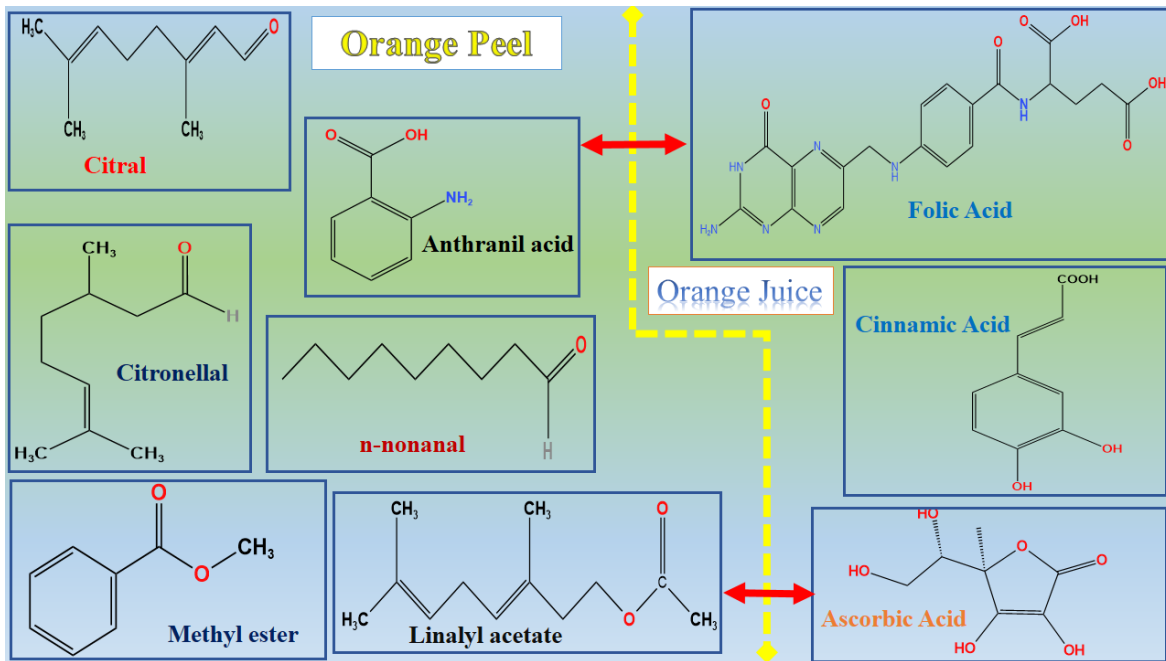
747

748

749

Supplementary Data

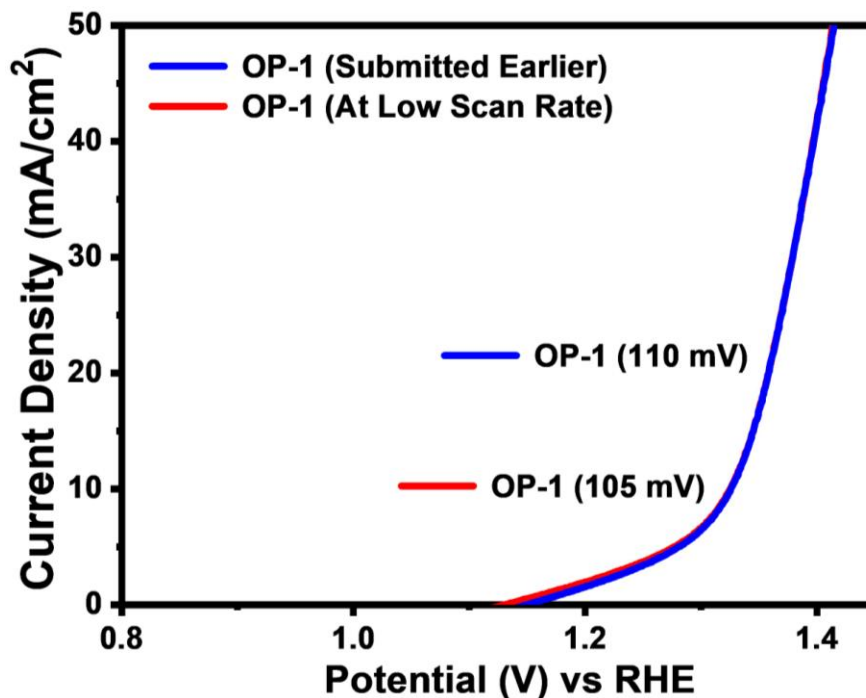
750



752 **Scheme 1:** Main molecular representation of chemical compounds existing in orange peel extract and
 753 its fruit juice.

761 **Scheme 3:** Proposed charge storage mechanism using NiCo₂O₄ nanostructures prepared with
762 orange peel extract and its fruit juice

763



764

765 **Figure 1:**

766

767

768 Table 1 contains detailed information about all the supercapacitor results.

769 The electrochemical supercapacitor performance of Op-1 was also evaluated and found to be
770 superior to recent reports (Table 2).

771

772 We also compared the OER performance with reported electrocatalysts based on NiCo₂O₄
773 nanostructures, its composites, and other materials, as shown in Table 3. The comparison
774 reveals that the presented electrocatalyst based on NiCo₂O₄ nanostructures prepared with
775 orange peel extract has superior performance in terms of low cost, easy synthesis, high
776 efficiency, and eco-friendliness.

777

778 In Scheme 1, a range of chemical constituents are presented using molecular structure
779 diagrams to illustrate their presence in orange peel extract and juice.

780 Briefly, the morphological transformation is illustrated in the Scheme 2.

781

782 **Table 1:** Calculated different performance evaluation parameters of proposed supercapacitors

Samples	Current Density (Ag⁻¹)	Specific Capacitance (Fg⁻¹)	Energy Density (Wh kg⁻¹)	Power Density (W kg⁻¹)	Columbic Efficiency (%)	Capacitance Retention (%)
OP-1	1.5	997.50	22.17	300	96%	100% - 96%
	2	780.00	17.33	400	(30000 Cycles)	(30000 Cycles)
	2.5	687.50	15.28	500		
	5	637.50	14.17	1000		
	10	525.00	11.67	2000		
OP-2	1.5	862.50	19.17	300		
OP-2	2	625.00	13.89	400	-	-
	2.5	537.50	11.94	500		
	5	512.50	11.39	1000		
	10	500.00	11.11	2000		
	Or-1	1.5	825.00	18.33		
Or-1	2	730.00	16.22	400	(30000 Cycles)	(30000 Cycles)
	2.5	581.25	12.92	500		
	5	562.50	12.50	1000		
	10	525.00	11.67	2000		
	Or-2	1.5	776.25	17.25		
Or-2	2	695.00	15.44	400	-	-
	2.5	543.75	12.08	500		
	5	525.00	11.67	1000		
	10	425.00	9.44	2000		
	Pure (NiCo₂O₄)	1.5	326.47	9.42		
Pure (NiCo₂O₄)	2	305.88	7.08	340	(30000 Cycles)	(30000 Cycles)
	2.5	250.00	6.61	425		

	5	235.29	6.14	850		
	10	205.88	5.67	1700		
Ni-Foam (Bare)	1.5	202.70	8.86	277	-	-
	2	194.59	6.78	370		
	2.5	162.16	6.17	462		
	5	148.65	5.65	925		
	10	135.14	5.14	1850		

783

784

785 **Table 2:** Comparative analysis of presented supercapacitor based on NiCo₂O₄ nanostructures
786 prepared with orange peel extract with recently reported results

Material	Specific Capacitance (F/g)	Current Density (A/g)	Potential Window (V)	Energy Density (Wh kg⁻¹)	Power Density (W kg⁻¹)	Reference
MWCNTs	84 F/g	0.6 A/g	-0.5 to 2.2 V	21	6237	[1]
NCO//MWCNT	157 F/g	0.6 A/g	-0.5 to 2.2 V	40	2816	[1]
NCO@MWCNT //MWCNT	242 F/g	0.6 A/g	-0.5 to 2.2 V	61	2837	[1]
NiCoF	50 F/g	1 A/g	0 to 1 V	-	-	[2]
NC6	1294 F/g	10 A/g	0.4 V	-	-	[3]
NC10	687 F/g	10 A/g	0.4 V	-	-	[3]
Ni-Co-O-1	568 F/g	20 A/g	0 to 0.5 V	19.72	5000	[4]
Ni-Co-O-2	532 F/g	20 A/g	-	-	-	[4]
NiCo₂O₄ (Lemon juice)	358 F/g	0.8 A/g	0 to 0.4 V	7.96	160	[5]
NiCo₂O₄ (Grapefruit)	434 F/g	0.8 A/g	0 to 0.4 V	9.64	160	[6]
<u>NiCo₂O₄ (OP-1)</u>	<u>997 F/g</u>	<u>1.5 A/g</u>	<u>0 to 0.4 V</u>	<u>22.17</u>	<u>300</u>	<u>This Work</u>

787

788

789

790 NiCo₂O₄ nanostructures, its composites, and other materials, as shown in Table 3. The
 791 comparison reveals that the presented electrocatalyst based on NiCo₂O₄ nanostructures
 792 prepared with orange peel extract has superior performance in terms of low cost, easy
 793 synthesis, high efficiency, and eco-friendliness.

794

795 **Table 3: OER comparative study of orange peel extract assisted NiCo₂O₄ nanostructures**

Catalyst	Over potential (mV) @ 10 mA/cm²	Electrolyte	References
CoS_x/MoS₂	347	1.0 M KOH	[7]
MOF derived-NiCo₂O₄/ NiO	430	1.0 M KOH	[8]
NiO_x/NiCo₂O₄/Co₃O₄	315	1.0 M KOH	[9]
NiCo₂O₄/CoO/graphite	323	1.0 M KOH	[10]
P-doped NiCo₂O₄ on Ni- Foam	300	1.0 M KOH	[11]
Co₈FeS₈/CoS@CNT	278	1.0 M KOH	[12]
CoxNi1-xS₂ (CNS)/rGO	290	1.0 M KOH	[13]
NiCo₂O₄/NiO	360	1.0 M KOH	[14]
NiCo₂O₄@Graphene nanosheets	383	1.0 M KOH	[15]
3D core-shell NiCo₂O₄@CoS/NF	290	1.0 M KOH	[16]
Grapefruit juice assisted NiCo₂O₄ material	260	1.0 M KOH	[17]
Sample 1 (Co₃O₄)	250	1.0 M KOH	[18]
<u>NiCo₂O₄ material (OP-1)</u>	<u>110</u>	<u>1.0 M KOH</u>	<u>This Work</u>

796

797

798

799 Reference

- 800 [1]. M. Pathak, J.R. Jose, B. Chakraborty, C.S. Rout, High performance supercapacitor
801 electrodes based on spinel NiCo₂O₄@ MWCNT composite with insights from density
802 functional theory simulations, *The Journal of Chemical Physics* 152 (2020) 064706.
- 803 [2] B. Bhujun, M.T. Tan, A.S. Shanmugam, Study of mixed ternary transition metal
804 ferrites as potential electrodes for supercapacitor applications, *Results in Physics* 7
805 (2017) 345-53.
- 806 [3] M. Kaur, P. Chand, H. Anand, Binder free electrodeposition fabrication of NiCo₂O₄
807 electrode with improved electrochemical behavior for supercapacitor application,
808 *Journal of Energy Storage* 52 (2022) 104941.
- 809 [4] H. Wang, Q. Gao, L. Jiang, Facile approach to prepare nickel cobaltite nanowire
810 materials for supercapacitors. *Small*. 7 (2011) 2454-2459.
- 811 [5] S. Kumar, A. Tahira, A.L. Bhatti, M.A. Bhatti, R.H. Mari, N.M. Shaikh, Z.H. Ibupoto,
812 Z. H. Transforming NiCo₂O₄ nanorods into nanoparticles using citrus lemon juice
813 enhancing electrochemical properties for asymmetric supercapacitor and water
814 oxidation. *RSC advances*. 13 (2023) 18614-18626.
- 815 [6] S. Kumar, A. Tahira, M. Emo, B. Vigolo, A. Infantes-Molin, A.M. Alotaibi, Z.H.
816 Ibupoto, Grapefruit juice containing rich hydroxyl and oxygenated groups capable of
817 transforming 1D structure of NiCo₂O₄ into 0D with excessive surface vacancies for
818 promising energy conversion and storage applications. *Journal of Energy Storage*. 68
819 (2023) 107708.
- 820 [7] L. Yang, L. Zhang, G. Xu, X. Ma, W. Wang, H. Song, D. Jia. Metal–Organic-
821 Framework-Derived Hollow CoS_x@ MoS₂ Microcubes as Superior Bifunctional
822 Electrocatalysts for Hydrogen Evolution and Oxygen Evolution Reactions, *ACS*
823 *Sustainable Chemistry & Engineering* 6 (2018) 12961-8.
- 824 [8] Y. Wang, Z. Zhang, X. Liu, F. Ding, P. Zou, X. Wang, H. Rao, MOF-derived
825 NiO/NiCo₂O₄ and NiO/NiCo₂O₄-rGO as highly efficient and stable electrocatalysts
826 for oxygen evolution reaction. *ACS Sustainable Chemistry & Engineering*. 6 (2018)
827 12511-12521.

- 828 [9] J. Chen, Y. Ling, Z. Lu, X. Huai, F. Qin, Z. Zhang, Sandwich-like
829 NiO_x/NiCo₂O₄/Co₃O₄ nanoflakes enable efficient oxygen evolution
830 electrocatalysis. *Electrochimica Acta*. 322 (2019) 134753.
- 831 [10] N. Srinivasa, L. Shreenivasa, P.S. Adarakatti, J.P. Hughes, S.J. Rowley-Neale, C.E.
832 Banks, S. Ashoka, In situ addition of graphitic carbon into a NiCo₂O₄/CoO
833 composite: enhanced catalysis toward the oxygen evolution reaction. *RSC advances*. 9
834 (2019) 24995-25002.
- 835 [11] W. Chu, Z. Shi, Y. Hou, D. Ma, X. Bai, Y. Gao, N. Yang, Trifunctional of
836 phosphorus-doped NiCo₂O₄ nanowire materials for asymmetric supercapacitor,
837 oxygen evolution reaction, and hydrogen evolution reaction. *ACS applied materials &*
838 *interfaces*. 12 (2019) 2763-2772.
- 839 [12] B. Wang, Y. Chen, X. Wang, X. Zhang, Y. Hu, B. Yu, W.A. Zhang, microwave-
840 assisted bubble bursting strategy to grow Co₈FeS₈/CoS heterostructure on rearranged
841 carbon nanotubes as efficient electrocatalyst for oxygen evolution reaction. *Journal of*
842 *Power Sources*. 449 (2020) 227561.
- 843 [13] Y.R. Hong, S. Mhin, K.M. Kim, W.S. Han, H. Choi, G. Ali, K.Y. Chung, H.J. Lee, S.I.
844 Moon, S. Dutta, S. Sun, Electrochemically activated cobalt nickel sulfide for an
845 efficient oxygen evolution reaction: partial amorphization and phase control, *Journal*
846 *of Materials Chemistry A*. 7 (2019) 3592-602.
- 847 [14] C. Mahala, M. Basu. Nanosheets of NiCo₂O₄/NiO as efficient and stable
848 electrocatalyst for oxygen evolution reaction. *ACS omega* 2 (2017) 7559-67.
- 849 [15] Li, Z.; Li, B.; Chen, J.; Pang, Q.; Shen, P. Spinel NiCo₂O₄ 3-D nanoflowers supported
850 on graphene nanosheets as efficient electrocatalyst for oxygen evolution
851 reaction. *International Journal of Hydrogen Energy*, 2019, 44, 16120-16131.
- 852 [16] S. Adhikari, Y. Kwon, D.H. Kim, Three-dimensional core-shell structured
853 NiCo₂O₄@ CoS/Ni-Foam electrocatalyst for oxygen evolution reaction and
854 electrocatalytic oxidation of urea, *Chemical Engineering Journal* 402 (2020) 126192.
- 855 [17] S. Kumar, A. Tahira, M. Emo, B. Vigolo, A. Infantes-Molin, A.M. Alotaibi, Z.H.
856 Ibupoto, Grapefruit juice containing rich hydroxyl and oxygenated groups capable of
857 transforming 1D structure of NiCo₂O₄ into 0D with excessive surface vacancies for
858 promising energy conversion and storage applications. *Journal of Energy Storage* 68
859 (2023) 107708.

860 [18] A.L. Bhatti, A. Tahira, S. Kumar, Z.A. Ujjan, M.A. Bhatti, Z.H. Ibupoto, Facile
861 synthesis of efficient Co₃O₄ nanostructures using the milky sap of *Calotropis*
862 *procera* for oxygen evolution reactions and supercapacitor applications. *RSC advances*
863 13 (2023) 17710-17726.
864